FIBROSIS

Copyright © 2019 The Authors, some rights reserved; exclusive licensee American Association for the Advancement of Science. No claim to original U.S. Government Works

Cadherin-11–mediated adhesion of macrophages to myofibroblasts establishes a profibrotic niche of active TGF-β

Monika Lodyga[1]*, Elizabeth Cambridge[1]*, Henna M. Karvonen[1,2], Pardis Pakshir[1,3], Brian Wu[4,5], Stellar Boo[1], Melanie Kiebalo[1], Riitta Kaarteenaho[2], Michael Glogauer[6], Mohit Kapoor[4,5], Kjetil Ask[7], Boris Hinz[1,2,6†]

Macrophages contribute to the activation of fibroblastic cells into myofibroblasts, which secrete collagen and contract the collagen matrix to acutely repair injured tissue. Persistent myofibroblast activation leads to the accumulation of fibrotic scar tissue that impairs organ function. We investigated the key processes that turn acute beneficial repair into destructive progressive fibrosis. We showed that homotypic cadherin-11 interactions promoted the specific binding of macrophages to and persistent activation of profibrotic myofibroblasts. Cadherin-11 was highly abundant at contacts between macrophages and myofibroblasts in mouse and human fibrotic lung tissues. In attachment assays, cadherin-11 junctions mediated specific recognition and strong adhesion between macrophages and myofibroblasts. One functional outcome of cadherin-11–mediated adhesion was locally restricted activation of latent transforming growth factor–β (TGF-β) between macrophage-myofibroblast pairs that was not observed in cocultures of macrophages and myofibroblasts that were not in contact with one another. Our data suggest that cadherin-11 junctions maintain latent TGF-β–producing macrophages and TGF-β–activating myofibroblasts in close proximity to one another. Inhibition of homotypic cadherin-11 interactions could be used to cause macrophage-myofibroblast separation, thereby destabilizing the profibrotic niche.

INTRODUCTION

Myofibroblasts (MFs) are activated in response to lung injury and inflammatory signals to repair damaged tissues by secreting and contracting collagenous extracellular matrix (ECM) (*1*–*3*). Acute inflammation and repair are normal healing responses to epithelium injury, but activated inflammatory cells, in particular macrophages, and MFs are gradually cleared once the repair of tissue architecture is underway. In contrast, the dysregulated chronic coexistence of macrophages with MFs is one condition that can convert beneficial acute tissue repair into persistent and destructive fibrosis (*4*–*9*). Lung fibrosis comprises the accumulation of stiff scar tissue in the delicate architecture of the lung, which obstructs and ultimately destroys lung function (*10*–*14*). An understanding of the mechanisms that promote the persistence of macrophages and MFs beyond normal repair is important for developing therapeutic interventions to prevent or reduce fibrosis. We here show that formation of cadherin-11 (CDH11)–mediated intercellular junctions retain macrophages in the vicinity of MFs, leading to prolonged MF activation by providing locally active transforming growth factor β1 (TGF-β1).

The adherens junction protein CDH11 (also called osteoblast cadherin or OB-cadherin) is predominantly present in mesenchymal cells (*15*–*17*), including embryonic fibroblasts (*18*), tendon cells (*19*), granulation tissue, lung and subcutaneous fibroblasts (*20*), synovial fibroblasts (*21*), cancer-associated fibroblasts, and tumor cells (*22*, *23*). We and others have previously established that CDH11 abundance increases during fibroblast-to-MF activation after treatment with TGF-β1 in culture and in the granulation tissue of healing wounds, in conjunction with production of the contractile MF marker α-smooth muscle actin (α-SMA) (*20*, *24*). CDH11 has since become a widely used marker for MFs in some normal tissues (*25*) and in various fibroproliferative conditions (*26*), including lung fibrosis (*27*, *28*), skin fibrosis (*29*), kidney epithelial-to-mesenchymal transition (*30*), calcific aortic stenosis (*31*, *32*), and Dupuytren disease (*33*). In addition, the presence of CDH11 is a hallmark of the proinflammatory phenotype of synovial fibroblasts in the context of arthritis (*34*).

More recently, the expression of *Cdh11* (mouse) and *CDH11* (human) and the presence of Cdh11 (mouse) and CDH11 (human) proteins were also documented in macrophages in fibrotic lung and skin (*27*, *29*), suggesting a functional role for CDH11 in conditions of fibrosis. Injury triggers the recruitment and activation of macrophages from circulating monocytes that originate in the bone marrow and extravasate at sites of injury (*35*–*38*). Activated macrophages have long been recognized as important producers of TGF-β1 (*35*, *39*–*42*), a cytokine that not only orchestrates normal healing but also drives fibrosis depending on the timing and location of TGF-β1 activation. Whereas macrophage recruitment is crucial for normal tissue repair, the persistence of macrophages beyond acute repair often contributes to excessive tissue repair and fibrosis (*36*, *43*, *44*). Inhibition or depletion of macrophages during fibrogenesis has been shown to reduce the extent of lung, liver, and skin tissue scarring (*45*–*49*). However, depletion of macrophages in the resolution phase of tissue repair can stimulate fibrosis, indicating that the timing and phenotype of macrophages are crucial (*48*, *50*).

[1]Laboratory of Tissue Repair and Regeneration, Faculty of Dentistry, University of Toronto, Toronto, Ontario M5G 1G6, Canada. [2]Respiratory Medicine, Research Unit of Internal Medicine, Medical Research Center Oulu, Oulu University Hospital and University of Oulu, POB 20, 90029, Oulu, Finland. [3]Institute of Biomaterials and Biomedical Engineering, University of Toronto, Toronto, Ontario M5S 3G9, Canada. [4]Department of Surgery and Department of Laboratory Medicine and Pathobiology, University of Toronto, Toronto, Ontario M5T 2S8, Canada. [5]Arthritis Program, Krembil Research Institute, University Health Network, Toronto, Ontario, Canada. [6]Faculty of Dentistry, University of Toronto, Toronto, Ontario M5G 1G6, Canada. [7]Department of Medicine, McMaster University, Firestone Institute for Respiratory Health, Hamilton, Ontario L8N 4A6, Canada.
*These authors contributed equally to this work.
†Corresponding author. Email: boris.hinz@utoronto.ca

Downloaded from http://stke.sciencemag.org/ on January 15, 2019

In addition to pathologic macrophage retention, dysregulated macrophage activation (polarization) is involved in tipping the balance between beneficial and detrimental repair. A shift from "classically activated" inflammatory M1 macrophages to "alternatively activated" macrophages, which have also been termed profibrotic, or remodeling M2 macrophages occurs as tissue repair progresses from an inflammatory to a restorative state (*36*, *51*). Although M1- and M2-polarized macrophages have been categorized on the basis of specific molecular markers and functions in vitro, macrophages are increasingly recognized to exist in a broader, more complex spectrum of activation states with specific functions in vivo (*52*–*58*). Whether CDH11 production depends on macrophage activation and polarization and the functional consequences of CDH11 presence in macrophage for the fibrotic microenvironment has not been investigated.

Because CDH11 is present in both MFs and macrophages under fibroproliferative conditions and because CDH11 on the surface of one cell can bind to CDH11 on a neighboring cell (homotypic binding) (*59*, *60*), we hypothesized that CDH11 mediates the direct adhesion of macrophages to fibroblastic cells. We show that CDH11 was indeed absent from normal parenchyma in human and mouse lungs but localized between macrophages and MFs within fibrotic foci, which are aggregates of fibroblastic cells and ECM proteins surrounded by hyperplastic alveolar epithelium. The abundance of CDH11 positively correlated with profibrotic activation of both fibroblasts and macrophages and mediated strong and specific heterocellular binding in vitro. The main functional consequence of CDH11 in the macrophage-MF pairs appeared to be in maintaining proximity for the effective delivery and activation of macrophage-produced TGF-β1 to MFs, the persistent activation of which depends on a continuous supply of TGF-β1. Through this mechanism of attaching TGF-β1–producing macrophages to TGF-β1–receiving MFs, we propose that CDH11 supports the chronic coexistence and continued activation of both cell types, culminating in fibrosis.

RESULTS

CDH11 is enriched between macrophages and MFs in human and mouse fibrotic lung tissue

We previously reported that Cdh11 protein abundance increases as part of the MF activation program during the healing of rat skin wounds (*20*). Subsequent studies reported the presence of CDH11 in fibroblasts and macrophages in human lung and skin fibrotic lesions (*27*, *29*). However, it has not been investigated whether CDH11 mediates heterotypic interactions between macrophages and MFs in fibrosis. In biopsies taken from histologically non-fibrotic but inflamed regions of the lungs of two patients with idiopathic pulmonary fibrosis (IPF), few alveolar cells were positive for the macrophage marker cluster of differentiation 206 (CD206) (Fig. 1A) or positive for both CDH11 and the macrophage marker CD68 (Fig. 1B). Patient-matched fibrotic regions of the same lung showed a large number of cells positive for CD206 or doubly positive for CD68 and CDH11 (Fig. 1, A and B). In cross sections of normal non-fibrotic human lung tissue, CDH11 was absent from the tissue and not present on CD68-positive alveolar macrophages (Fig. 1C). In fibrotic foci in the lungs of patients with IPF, CDH11 was present on both CD68-positive macrophages and α-SMA stress fiber–positive MFs and localized to areas of contact between adjacent cells (Fig. 1, C and D). Analysis of publicly available datasets showed that *CDH11* expression was increased in early IPF lung tissue compared to non-fibrotic control and advanced IPF tissues (Fig. 1E) (*61*). *CDH11* was also more highly expressed in lung tissue from patients with IPF compared to lung tissue from patients with other interstitial lung diseases and to normal lung tissue (Fig. 1F) (*62*). These patterns are consistent across species because *Cdh11* expression increased upon bleomycin-induced lung fibrosis in rat (*63*) and mouse (*64*) models (Fig. 1G). In rodents, *Cdh11* expression peaked after 1 to 2 weeks of experimentally induced fibrosis, after which *Cdh11* expression returned to an amount comparable to mock-treated animals (Fig. 1G). In a mouse model of induced lung fibrosis, $CD68^+$ macrophages accumulated 7 days after administration of bleomycin, coinciding with the onset of increased Cdh11 production and high α-SMA abundance (Fig. 2A). Although the overall amount of CD68 decreased in severe fibrosis after 21 days (Fig. 2A), the remaining macrophages accumulated Cdh11 in the vicinity of Cdh11-positive MFs (Fig. 2, B and C). Together, these experimental results and meta-analyses demonstrate that the production of CDH11 increases early during the onset of lung fibrosis in both macrophages and MFs.

CDH11 junctions have not been previously reported to exist between macrophages and MFs. To test whether Cdh11 plays a functional role in physically coupling macrophages and MFs, we isolated macrophages from mouse lung tissue 7 days after instillation of bleomycin (fibrosis) or saline as a control (Fig. 2D). Alveolar macrophages were collected first by BAL, and then, interstitial macrophages were collected by digesting lung tissue and selecting for CD45 and CD64 double-positive cells by fluorescence-activated cell sorting (FACS) (Fig. 2E). Bleomycin treatment resulted in increased percentages of CD45 and CD64 double-positive macrophages in the population of all extracted cells compared to saline controls (Fig. 2F, inset). Although the induction of fibrosis did not alter *Cdh11* mRNA abundance in alveolar macrophages compared to cells from control animals, *Cdh11* expression in interstitial macrophages isolated from bleomycin-treated lungs was 20-fold higher than in cells isolated from saline-treated controls (Fig. 2F). $Cdh11^{high}$ interstitial macrophages that were seeded onto monolayers of cultured primary mouse lung fibroblasts (mLFs) stained positive for Cdh11 that accumulated in junctions between α-SMA–positive MFs and heterocellular junctions between macrophages and MFs (Fig. 2G).

Because surface proteins are prone to degradation during the isolation procedure, we used alternate methods to establish cultures of primary mouse fibroblasts (fig. S1) from lung tissue and macrophages from bone marrow (fig. S2) that were more amenable for functional studies. Primary fibroblasts explanted from mouse lungs spontaneously activate to become α-SMA–positive MFs in standard culture. To generate populations with low abundance of α-SMA, we subcultured lung fibroblasts on normal lung-soft culture dishes (5-kPa elastic modulus) (*65*) in the presence of the TGF-β receptor inhibitor (SB431542) for one passage. Under these conditions, only about 25% of the cells differentiated into MFs (fig. S1). If the cells were plated on a stiff substrate in the presence of active TGF-β1 for one passage, then 85% of the cells differentiated into MFs (Fig. 3A and fig. S1). All subsequent experiments were performed on standard stiff culture plastic in standard culture medium for up to 4 days, during which α-SMA–low fibroblasts and α-SMA–high MFs maintained their pre-induced phenotype. We derived primary macrophages from mouse bone marrow monocytes stimulated with macrophage colony-stimulating factor (M-CSF), followed by in vitro activation with lipopolysaccharide (LPS), which promotes M1 macrophage polarization, or interleukin-4 (IL-4) plus IL-13, which promotes M2

Downloaded from http://stke.sciencemag.org/ on January 15, 2019

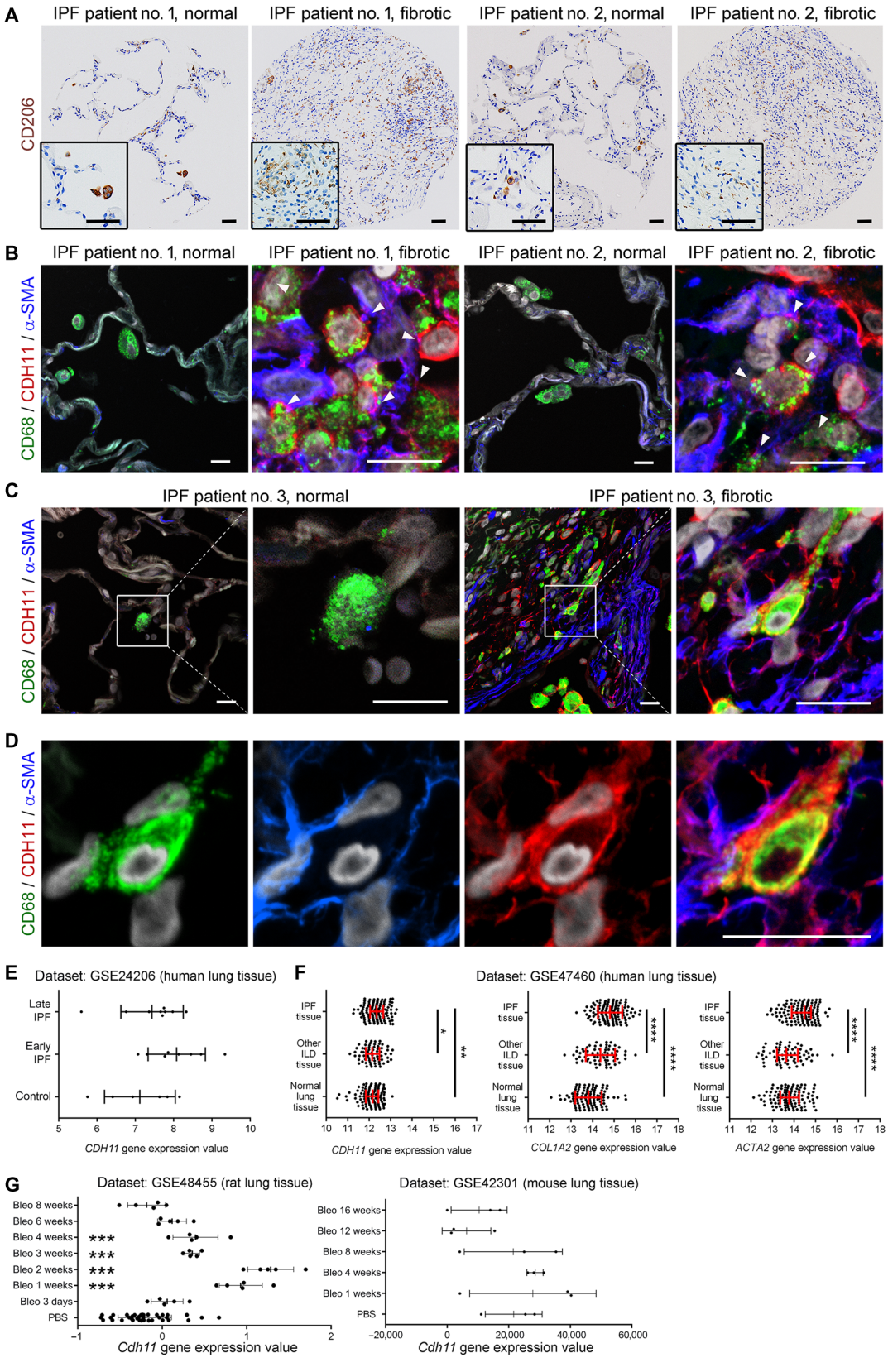

Fig. 1. CDH11 is present at contacts between macrophages and MFs in fibrotic human lungs. (**A**) Representative immunohistological staining for the macrophage marker CD206 (brown) on histological sections of lung from patients with IPF in unaffected lung regions ("normal") and regions classified by a pathologist as fibrotic from the same patient. Select regions are shown in high magnification insets. Scale bars, 50 μm. (**B**) Confocal fluorescence imaging corresponding to a consecutive slice of the samples shown in (A), immunolabeled for the macrophage marker CD68, the MF marker α-SMA, and CDH11. Cell nuclei are white [4′,6-diamidino-2-phenylindole (DAPI)]. Arrowheads point to CDH11 signals between CD68-positive macrophages and α-SMA–positive MFs. Scale bars, 20 μm. (**C**) Confocal fluorescence imaging of histological sections of two additional patients with IPF in unaffected lung regions (normal) and regions classified by a pathologist as fibrotic from the same patient. Sections are immunolabeled to show CD68, α-SMA, and CDH11. Cell nuclei are white. Scale bars, 20 μm. (**D**) The boxed region of the fibrotic sample from IPF patient no. 3 is shown at higher magnification with channels separated and merged. Scale bars, 20 μm. (**E**) Data for *CDH11* mRNA expression extracted from the Gene Expression Omnibus (GEO) microarray database, comparing whole extracts of lung tissue from human patients diagnosed with early IPF ($n = 8$) and late IPF ($n = 9$) and from control subjects ($n = 6$) (GEO Dataset Series, GSE24206). (**F**) Data for *CDH11* mRNA expression extracted from the GEO microarray database, comparing whole extracts of lung tissue from human patients diagnosed with IPF ($n = 124$) and other interstitial lung diseases (ILD) ($n = 124$) and from control subjects ($n = 108$) (GSE47460). (**G**) Data for *CDH11* mRNA expression extracted from the GEO microarray database, comparing whole extracts of lung tissue from bleomycin-induced lung fibrosis in rat ($n = 5$ animals per bleomycin-treated group and $n = 37$ for saline controls) and mouse ($n = 3$ animals per group) animal studies. Gene expression value distributions are shown as means ± SD [$^{*}P < 0.05$, $^{**}P < 0.01$, $^{***}P < 0.001$, and $^{****}P < 0.0001$, analysis of variance (ANOVA) with Kruskal-Wallis multiple comparisons test]. PBS, phosphate-buffered saline.

Downloaded from http://stke.sciencemag.org/ on January 15, 2019

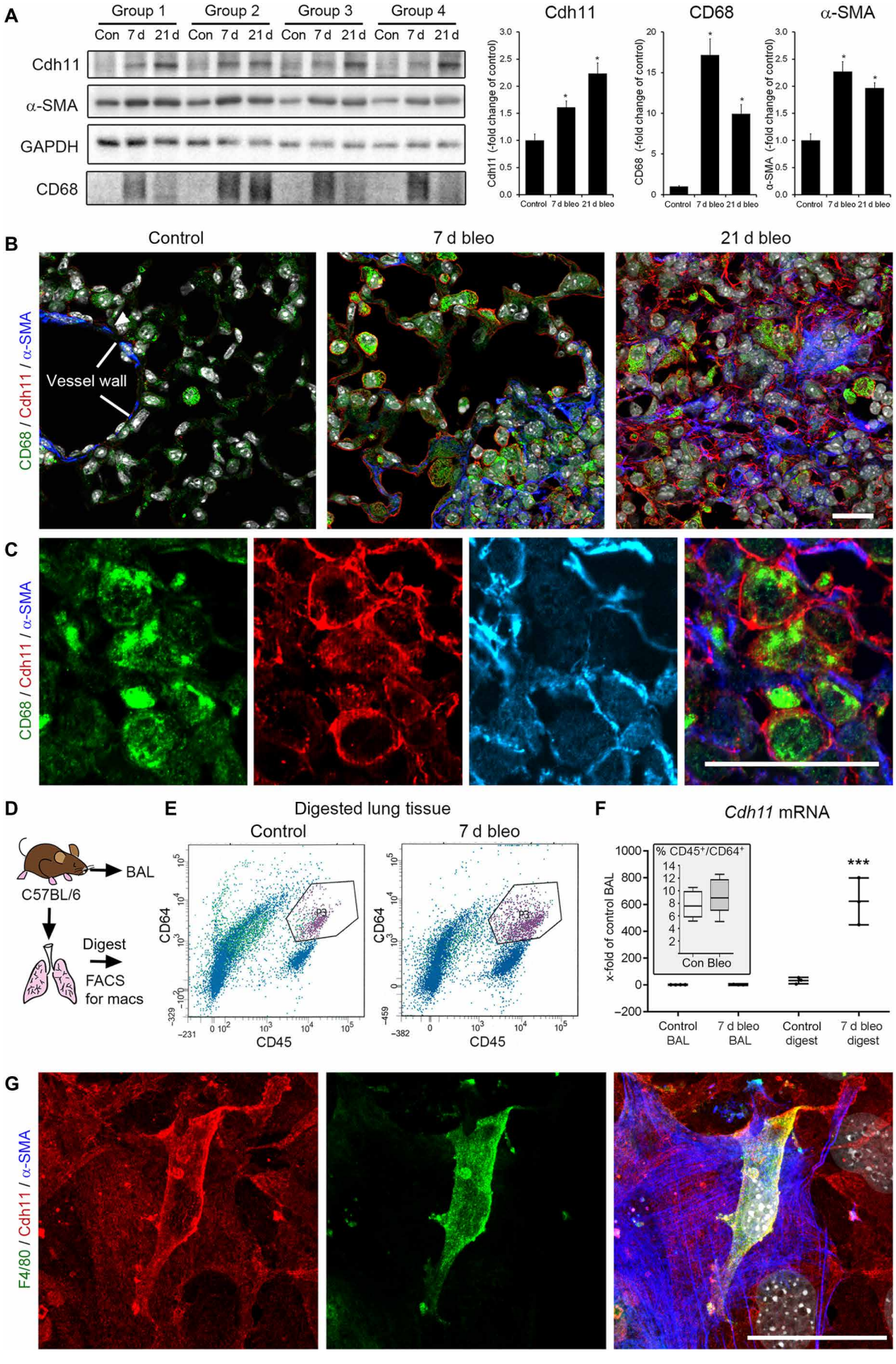

Fig. 2. Cdh11 is present between macrophages and MFs in fibrotic mouse lungs. (**A**) Western blotting of extracts of lung tissue from C57BL/6 mice 7 or 21 days after intratracheal instillation of bleomycin or saline controls for 21 days (con). Blots were probed to detect α-SMA, Cdh11, CD68, and the loading control glyceraldehyde-3-phosphate dehydrogenase (GAPDH). Protein quantifications were first normalized to GAPDH and then to saline controls. Graphs show means ± SD of $n = 4$ animals per time point per group (total = 12 animals; $^*P \leq 0.05$, Student's t test). (**B**) Representative confocal immunofluorescence showing the macrophage marker CD68, the MF marker α-SMA, and Cdh11 in paraffin-embedded sections of mouse lung tissues. Cell nuclei are white (DAPI). (**C**) Higher magnification view of a tissue section from bleomycin-treated mice 21 days after treatment. (**D**) Alveolar macrophages were isolated from mice by bronchoalveolar lavage (BAL) and interstitial by digestion of lung tissue and cell sorting. (**E**) Flow cytometry and sorting of interstitial macrophages for CD45 and CD64 7 days after instillation of bleomycin or saline (control). The CD45/CD64 double-positive cells in the outlined region were purified. (**F**) Quantification of *Cdh11* expression in alveolar (BAL) and sorted interstitial CD45/CD64 double-positive (digest) macrophages. The inset shows the percentages of CD45/CD64 double-positive cells among all the digested cells in box plot (median, minimum, and maximum). *Cdh11* quantification is shown as means ± SD of at least three samples, each pooled from three to four mice. $^{***}P < 0.001$, ANOVA with Dunnett's multiple comparisons test. (**G**) Representative confocal section showing CD45/ CD64 double-positive interstitial macrophages sorted from fibrotic mouse lung and directly seeded on top of primary lung fibroblast monolayers. Immunostaining shows the macrophage marker F4/80, α-SMA, and Cdh11. Cell nuclei are white. Scale bars, 50 μm.

Downloaded from http://stke.sciencemag.org/ on January 15, 2019

macrophage polarization (Fig. 3B and fig. S2A). The resulting in vitro macrophage populations attained robust and distinct "proinflammatory" (M1) and "profibrotic" or "regenerative" (M2) features and functions. Although the relevance of the M1 and M2 macrophage classifications in vivo is still an area of active investigation (*52*, *66*), we adopted the M1 and M2 macrophage terminology in vitro for reasons of simplicity. Cultured mouse M1 macrophages (LPS) were positive for mouse macrophage marker F4/80, CD68, inducible nitric oxide synthase (iNOS), expressed abundant T lymphocyte activation antigen CD80, and various proinflammatory cytokines characteristic of M1-type macrophages but had low amounts of mannose receptor CD206 (Fig. 3B and fig. S2, B to E). M2 macrophages (IL-4 and IL-13) expressed low amounts of CD80 and no iNOS but were positive for F4/80, CD68, arginase-1 (Arg-1), abundant CD206, and various profibrotic cytokines characteristic of M2-type macrophages (Fig. 2B and fig. S2, B to E). Stimulation of profibrotic features enhanced Cdh11 protein abundance in both fibroblastic cells and macrophages (Fig. 3, A and B).

MFs and macrophages form functional CDH11-positive adherens junctions

M2 macrophages costimulated with IL-4 and IL-13 produced the greater amounts of CDH11 and the adherens junction proteins β-catenin and α-catenin than in vitro LPS-polarized M1 macrophages (Fig. 3, A and B). When M2 macrophages were directly seeded onto monolayers of MFs, Cdh11 was enriched in discrete striae in the macrophage periphery at the interface with MFs, as observed by confocal immunofluorescence (Fig. 3C). Contact points between MFs and M2 macrophages were characterized by submembranous electron-dense actin bundles reminiscent of adherens junctions in transmission electron microscopy (Fig. 3D). At these macrophage-MF contact points, plasma membranes were positive for immunogold-labeled Cdh11 in electron microscopy cryosections (Fig. 3E). Collectively, these findings demonstrate the existence of Cdh11-containing junctions between macrophages and MFs.

To test whether the different amounts of Cdh11 present in in vitro–polarized M1 and M2 macrophages associated with altered adhesion to fibroblastic cells, we performed a battery of assays measuring different cell adhesion properties and functions of the cells. Three hours after seeding in vitro–polarized macrophages onto confluent monolayers of MFs, $Cdh11^{high}$ M2 macrophages adhered to the MFs at a greater frequency (twofold higher numbers of cells adhered) and with greater cell spreading than $Cdh11^{low}$ M1 macrophages (Fig. 4, A and B). M2 macrophages exhibited twofold larger spreading area when attaching to $Cdh11^{high}$ MFs than to $Cdh11^{low}$ fibroblasts (Fig. 4C). In heterocellular suspension aggregation assays, the number of M2 macrophages forming aggregates with MFs was twofold higher than those forming aggregates with fibroblasts, indicating higher surface affinity between the two $Cdh11^{high}$ cell populations (Fig. 4D). To assess the strength of macrophage-MF adhesions, M2 macrophages were attached to fibroblast and MF monolayers in a fluid flow chamber setup and subjected to gradually increasing shear stress. After weakly adherent M2 macrophages were eliminated using low shear stress (1.1 $N/\mu m^2$), the numbers of M2 macrophages remaining attached to MFs were two to four times higher than the numbers remaining attached to fibroblasts, with the maximum difference between adherence to MFs and adherence to fibroblasts at the highest stress tested (fourfold at 5.5 $N/\mu m^2$) (Fig. 4E).

We repeated adhesion tests in the presence of the Cdh11 function–blocking antibodies 23C6 and 13C2, which were previously developed and characterized to block mouse Cdh11 in vivo and in vitro (*21*, *27*, *29*). Blocking the function of Cdh11 resulted in a twofold reduction in the number of strongly adherent M2 macrophages on MF monolayers under high shear force compared to isotype controls (Fig. 4F). Cdh11 homodimerization is calcium-dependent, and chelation of extracellular calcium with EGTA completely eliminated adhesion of M2 macrophages to MFs (Fig. 4G). Moreover, we observed a fourfold reduction in M2 macrophage spreading area on MF monolayers (Fig. 4H) and a twofold reduction in M2 aggregation with MFs (Fig. 4I) in the presence of Cdh11 function–blocking antibodies as compared to the IgG controls. To test whether antibody-mediated inhibition of Cdh11 generally disrupted adhesion to any surface, we incubated MF and macrophage monocultures during cell plating with the Cdh11-blocking antibody 23C6. Treatment with 23C6 inhibited the formation of Cdh11-positive adherens junctions between MFs, as expected (Fig. 4J), but did not interfere with the attachment of MFs (Fig. 4J) or M1 or M2 macrophages (Fig. 4K) to the plastic surface of the culture dish. Control IgG antibodies did not affect cell-cell or cell-plate adhesions (Fig. 4, J and K). Collectively, these results demonstrated that M2 macrophages and MFs form Cdh11-containing junctions in vitro that promote strong heterocellular adhesion and specific recognition.

Direct contact with macrophages enhances MF activation

Macrophages are considered to be crucial for MF activation in wound healing and fibrosis (*4*, *67*). To test whether the formation of junctions with macrophages affects MF activation, we established cocultures of M2 macrophages with fibroblasts in which the two cell types were either in direct contact or physically separated but shared the same culture medium (Fig. 5A). The percentage of α-SMA–positive cells (MFs) in segregated cocultures of fibroblasts and M2 macrophages was low, similar to the percentage of α-SMA–positive cells in fibroblast monocultures (25%) (Fig. 5B). Direct coculture of M2 macrophages with fibroblasts resulted in a threefold increase in the percentage of cells differentiated into α-SMA–positive MFs (75%), which was comparable to fibroblasts cultured alone in the presence of active TGF-β1 (85%). The MF-activating effect of allowing direct contact with macrophages was abolished by inhibiting TGF-β with soluble recombinant TGF-β receptor type II (TGFRII-Fc) during the coculture period (Fig. 5B). In addition to stimulating α-SMA production, the presence of M2 macrophages increased the percentage of highly contractile fibroblastic cells from 30% (fibroblast monoculture) to 80% in direct coculture but not in segregated cocultures (25%) (Fig. 5C). Enhanced contraction, as quantified by visible deformations (wrinkles) created by fibroblasts on silicone substrates (*68*) was particularly enhanced when multiple M2 macrophages were spreading on the same fibroblastic cell (Fig. 5D). Macrophage-induced fibroblast contraction was comparable to the effect of adding active TGF-β1 to MF monocultures and was mitigated by inhibiting active TGF-β with TGFRII-Fc in MF-macrophage cocultures (Fig. 5, C and D). Because MF activation through direct contact with M2 macrophages depended on TGF-β, we next measured active TGF-β in the cocultures by adding active TGF-β–reporting mink lung epithelial cells (TMLCs) to each of the different culture setups (fig. S3A). Direct M2 macrophage–fibroblast cocultures exhibited higher amounts of active TGF-β compared to segregated cocultures of cultures of fibroblasts alone (twofold) (Fig. 5E). TGFRII-Fc inhibited

Downloaded from http://stke.sciencemag.org/ on January 15, 2019

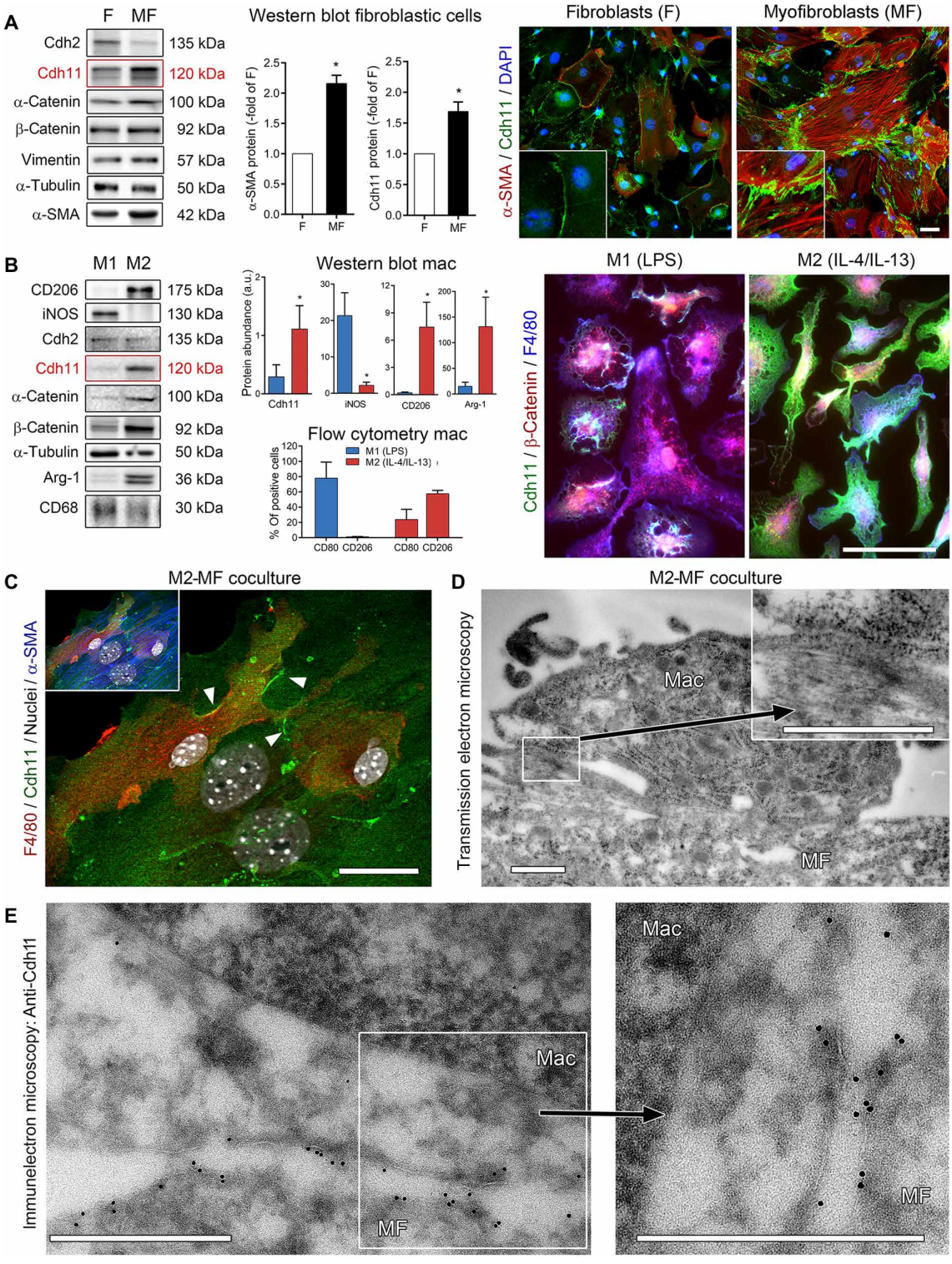

Fig. 3. Cdh11 localizes to heterocellular junctions between mLFs and in vitro–activated macrophages. (**A**) Immunoblotting and immunofluorescence microscopy of mLFs treated with the TGF-β receptor inhibitor SB431542 on lung-soft substrates (fibroblasts, F) or with TGF-β1 on stiff substrates (MF). Blot shows Cdh2, Cdh11, α-catenin, β-catenin, vimentin, α-tubulin, and α-SMA. The abundances of α-SMA and Cdh11 were quantified. The immunofluorescence images show Cdh11, α-SMA, and nuclei (DAPI). Protein quantifications were first normalized to vimentin and then to the amount present in fibroblasts. Graphs show means ± SD ($n = 3$ independent cultures; $^*P < 0.05$, Student's t test). (**B**) Characterization of primary macrophages from mouse bone marrow polarized using LPS to generate M1 macrophages or IL-4 and IL-13 to generate M2 macrophages. The Western blot shows Cdh2, Cdh11, α-catenin, β-catenin, α-tubulin, CD68, the M1-specific marker iNOS, and the M2-specific markers CD206 and Arg-1 in M1 and M2 macrophages polarized in vitro. The amounts of Cdh11, iNOS, CD206, and Arg-1 in each cell type were quantified. In vitro–polarized M1 and M2 macrophages were sorted by FACS for CD80, which is high in M1 macrophages and low in M2 macrophages, and CD206. Immunofluorescence images show Cdh11, β-catenin, and the macrophage marker F4/80 in M1 and M2 in vitro–polarized macrophages. Protein quantifications were normalized to α-tubulin. Graphs show means ± SD of $n = 3$ independent experiments with cells from at least three animals ($^*P \leq 0.05$, using ANOVA followed by a post hoc Tukey's multiple comparisons test). (**C**) Representative confocal micrographs of in vitro–polarized M2 macrophages seeded onto confluent monolayers of MFs. Cdh11-containing junctions (green) between macrophages (F4/80, red) and MFs (α-SMA, inset and blue) were resolved in one optical section (0.5 μm) at the cell-cell interface. (**D**) Representative transmission electron micrographs showing enrichment of actin at sites of intercellular adherens junctions between in vitro–polarized M2 macrophages grown on top of MFs. (**E**) Immunoelectron microscopy showing Cdh11 localization at heterocellular (macrophage-MF) contacts. $n = 3$ independent cultures from at least three different animals. Scale bars, 25 μm (A to C) and 500 nm (D to E).

Downloaded from http://stke.sciencemag.org/ on January 15, 2019

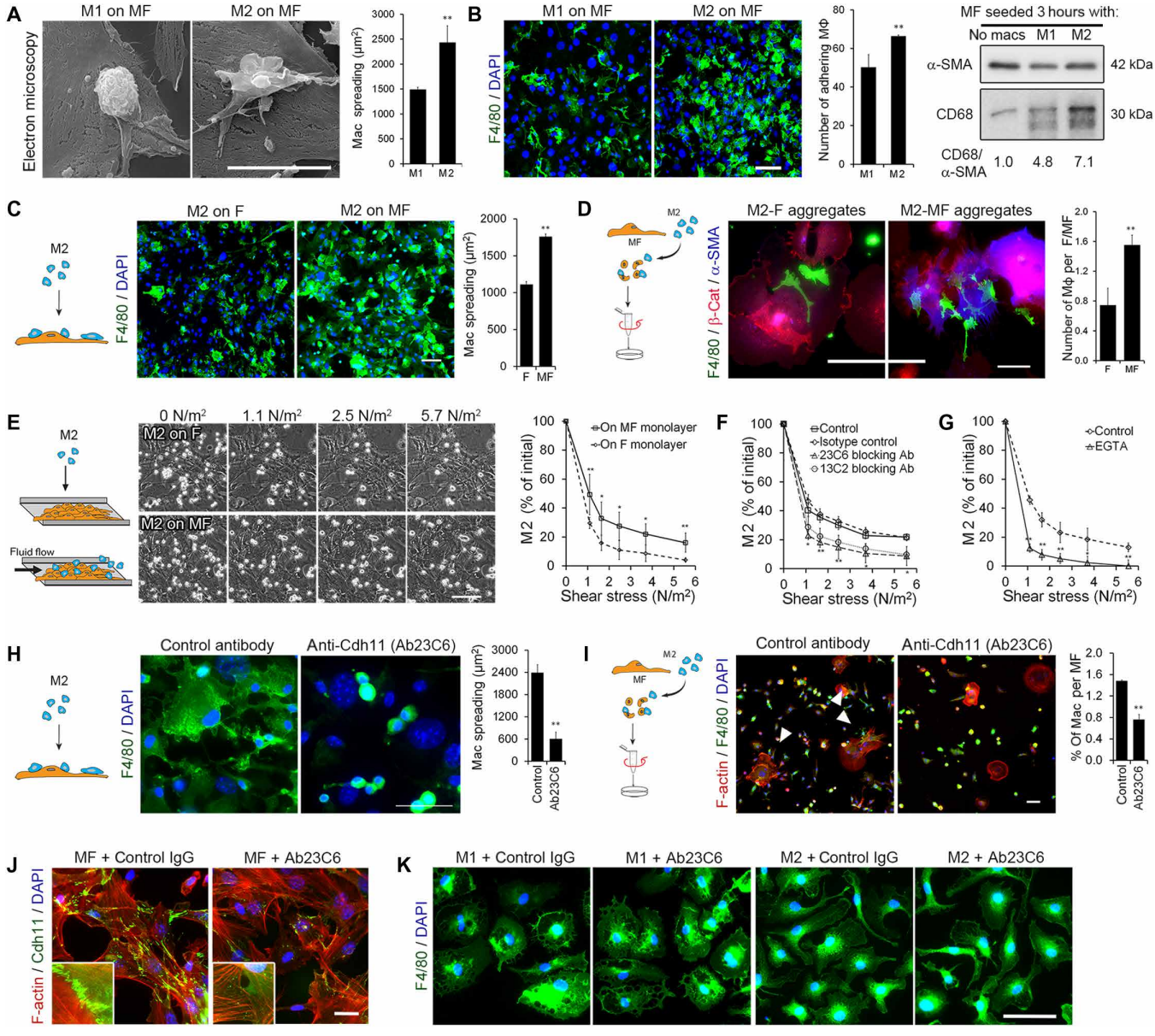

Fig. 4. Functional Cdh11 adhesions mediate heterocellular interactions between macrophages and MFs. (**A**) Scanning electron microscopy showing M1 and M2 macrophage adhesion to and spreading on confluent MF monolayers, after jet washing of low-adherent macrophages. (**B**) Immunofluorescence images show the macrophage marker F4/80 and nuclei (DAPI), which were used to quantify the numbers and average spreading areas of macrophages adhering to MFs. The Western blot shows the macrophage marker CD68, the MF marker α-SMA, and the relative abundances of these proteins in M1 and M2 macrophages seeded with MFs. The ratios of CD68 to α-SMA were calculated from $n = 3$ independent experiments. (**C**) Immunofluorescence microscopy of in vitro–polarized M2 macrophages seeded onto fibroblast (F) or MF monolayers and washed to remove low-adherent macrophages. F4/80 and nuclei were used to quantify the average macrophage spreading area. (**D**) Immunofluorescence microscopy of aggregates formed by suspended M2 macrophages with either fibroblastic or MF cells. β-Catenin, F4/80, and α-SMA were used to quantify the percentage of cells in aggregates that were macrophages. (**E**) Heterocellular attachment strength was assessed by seeding M2 macrophages onto fibroblasts and MF monolayers in a fluid flow chamber, removing weakly attached macrophages using low (1.1 N/m^2) shear stress, and then gradually increasing the shear stress in steps of 1 N/m^2 every 30 s. The macrophages (bright and circular) remaining after each step were quantified from phase-contrast images by automated image analysis and plotted as a function of shear stress. (**F** and **G**) Fluid flow chamber adhesion tests were also performed in the presence of the Cdh11 function–blocking antibodies (Abs) 23C6 and 13C2 or immunoglobulin G (IgG) control antibodies (F) and in the presence of the calcium chelator EGTA (G). (**H** and **I**) Jet-wash (H) and aggregation (I) assays with M2 macrophages and MFs were performed in the presence of Cdh11 function–blocking antibody 23C6 or IgG control. (**J**) Immunofluorescence microscopy showing F-actin, Cdh11, and nuclei of MFs plated on tissue culture plastic in the presence of the Cdh11 function–blocking antibody 23C6 or the IgG control antibody. The insets show cell junctions in higher magnification. (**K**) Immunofluorescence microscopy showing F4/80 and nuclei of macrophages plated on plastic tissue culture dishes in the presence of the Cdh11 function–blocking antibody 23C6 or IgG control antibody. Representative images from $n = 3$ independent experiments. All graphs show means ± SD from $n = 3$ independent experiments with cells from at least three animals (*$P \leq 0.05$ and **$P \leq 0.01$, using ANOVA followed by a post hoc Tukey's multiple comparisons test). Scale bars, 50 μm.

Downloaded from http://stke.sciencemag.org/ on January 15, 2019

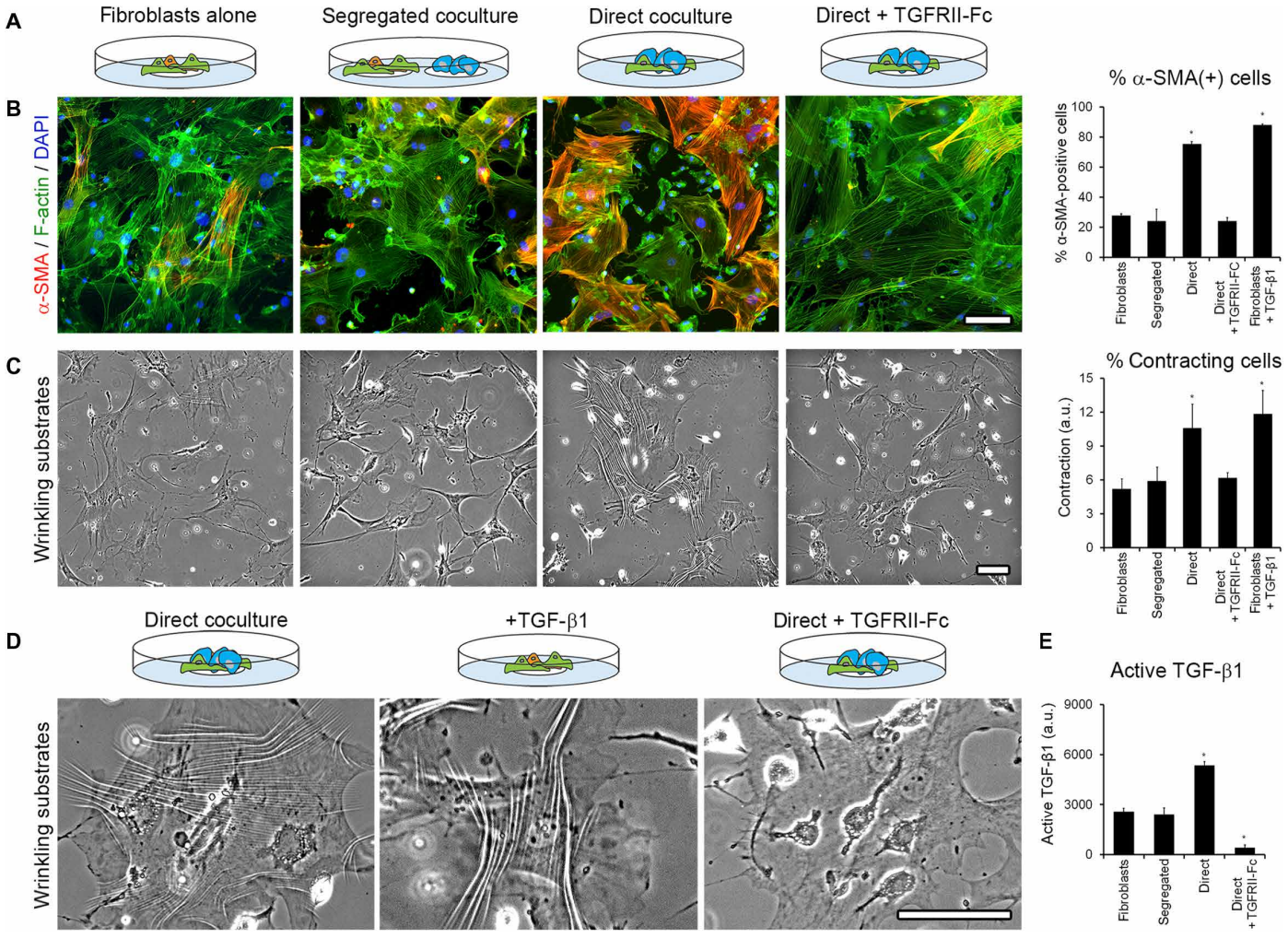

Fig. 5. Direct contact is required for macrophage-induced fibroblast-to-MF activation. (**A**) In plastic dishes with custom-made wells that allowed for different populations of cells to share the same medium without contacting one another, mLFs were cultured alone, in segregated cocultures with in vitro–polarized M2 macrophages, or in direct contact with in vitro–polarized M2 macrophages in the absence or presence of the TGF-β1 inhibitor TGFRII-Fc. (**B**) Immunofluorescence images showing α-SMA, F-actin (phalloidin), and nuclei (DAPI) in each of the culture conditions in (A). The percentages of cells that were α-SMA–positive–activated MFs in each condition were quantified by image analysis. (**C**) Phase-contrast microscopy of cells cultured as in (A) on a deformable silicone substrate to show and quantify high cell force exertion (contraction), as indicated by the formation of wrinkles in the substrate. (**D**) High magnification micrographs of mLFs and in vitro–polarized M2 macrophages on silicone substrates in direct coculture, fibroblasts alone in the presence of active TGF-β1, and in direct coculture in the presence of soluble recombinant TGFRII-Fc. (**E**) Triple coculture assays were performed with mLFs, in vitro–polarized M2 macrophages, and TMLC reporter cells to measure TGF-β1–dependent luciferase reporter activity. All graphs show means ± SD from $n = 3$ independent experiments performed with cells from at least three animals (*$P \leq 0.05$, using ANOVA followed by a post hoc Tukey's multiple comparisons test). Scale bars, 75 μm.

the TMLC response in direct cocultures, demonstrating that the activity of the reporter cells was specific for TGF-β (Fig. 5E).

These results could be interpreted to mean that the baseline production of TGF-β by macrophages alone is low but increases when they are in direct contact with fibroblasts. TMLCs cultured in the presence of conditioned supernatants from in vitro–polarized macrophage cultures or directly cocultured with macrophages did not report any active TGF-β (Fig. 6A). TGF-β remains latent after secretion because of sequestration into complexes with other proteins, and heat-treating supernatants or cell lysates can release active TGF-β molecules (fig. S3) (*69*). TMLCs incubated with heat-activated macrophage-conditioned supernatants and macrophage lysates reported 20 to 50 times higher amounts of TGF-β compared to the amounts present in native (not heat-activated) supernatants and cells, with little difference between the M2 and M1 macrophages (Fig. 6B). Consistent with macrophages producing latent TGF-β, treatment of fibroblast cultures with macrophage-conditioned supernatant alone did not increase the percentage of α-SMA–positive MFs over baseline (23%), whereas treatment with heat-activated macrophage supernatants and cells increased MF percentages two- to threefold (50 to 75%) (Fig. 6C). It is conceivable that engagement of Cdh11 receptors on the macrophage surface directly stimulates secretion or activation of TGF-β1. However, when macrophages were cultured alone on substrates coated with functional recombinant CDH11:human IgG-Fc (CDH11:Fc) fusion proteins (*60*), the amounts of total and active TGF-β1 measured with TMLCs did not differ from the amounts present in macrophage control cultures on fibronectin or noncoated substrates (Fig. 6, D and E). These results

Downloaded from http://stke.sciencemag.org/ on January 15, 2019

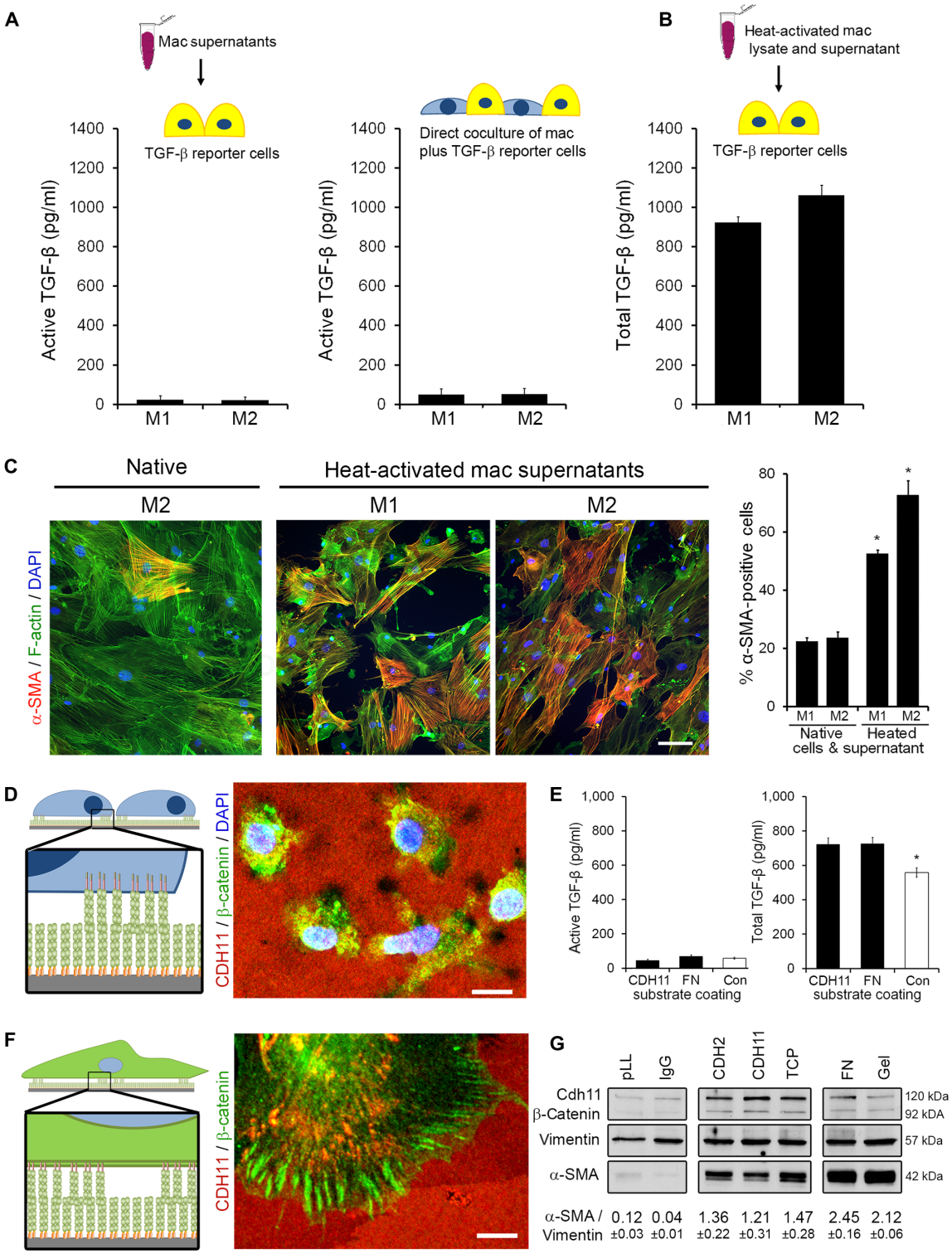

Fig. 6. Cultured macrophages produce but do not activate latent TGF-β1. (**A**) TGF-β–reporting TMLCs were used to measure the amounts of active TGF-β1 in macrophage-conditioned medium and in direct coculture with in vitro–polarized M1 and M2 macrophages. (**B**) Total (latent and active) TGF-β1 content of macrophages, as measured by incubating TMLCs with heat-activated macrophage culture supernatants plus cell lysates. (**C**) Immunofluorescence showing α-SMA, F-actin (phalloidin), and nuclei (DAPI) in fibroblasts incubated with native (not heat-activated) or heat-activated macrophage culture supernatants plus lysates. The percentage of α-SMA–positive–activated MFs was quantified for each condition. (**D**) In vitro–polarized M2 macrophages were cultured on substrates coated with recombinant CDH11:Fc fusion proteins and immunostained to show Cdh11, β-catenin (β-cat), and nuclei (DAPI). (**E**) TMLC reporter cells were used as in (A) and (B) to measure the amounts of total and active TGF-β1 in supernatants of macrophages on CDH11, fibronectin (FN), or uncoated (con) substrates. (**F**) Fibroblasts were cultured on substrates coated with recombinant CDH11:Fc fusion proteins and immunostained to show Cdh11 and β-catenin. (**G**) Western blots showing Cdh11, β-catenin (β-cat), vimentin (vim), and α-SMA in lysates from fibroblasts grown on substrates coated with poly-L-lysine (pLL), human IgG (IgG), CDH2:human IgG Fc fusion protein (CDH2), CDH11:Fc fusion protein (CDH11), tissue culture plastic (TCP), fibronectin (FN), or gelatin (gel). The ratio of the MF marker α-SMA to vimentin protein–loading control was quantified to evaluate MF activation on differently coated substrates. All graphs and Western blot quantification show means ± SD from $n = 3$ independent experiments performed with cells from at least three animals (*$P \leq 0.05$, using ANOVA followed by a post hoc Tukey's multiple comparisons test). All scale bars, 50 μm.

indicated that cultured macrophages produce high amounts of latent TGF-β1 that only becomes active and available to fibroblasts with direct coculture.

To test whether binding to CDH11 directly activates MFs, fibroblasts were grown for 4 days on CDH11:Fc-coated surfaces. Formation of β-catenin–positive focal adhesion–like attachments demonstrated

Downloaded from http://stke.sciencemag.org/ on January 15, 2019

proper engagement of Cdh11 on MFs by the human CDH11 fusion protein (6F), but α-SMA amounts were unchanged compared with cells grown on surfaces coated with CDH2:Fc (N-cadherin fusion proteins) or on noncoated surfaces (Fig. 6G). High α-SMA amounts on substrates coated with fibronectin or gelatin and low α-SMA amounts on substrates coated with poly-L-lysine or human IgG verified that fibroblasts were responsive to different substrates with respect to MF activation (Fig. 6G).

Next, we tested whether maintenance of MF activation depended on Cdh11 using a loss-of-function approach. To enhance knockdown efficacy, we created an mLF cell line by immortalizing primary cells using human telomerase reverse transcriptase (hTERT). We named the resulting cell line mLF-hT. Immortalized mLF-hT cells retained all characteristics of primary fibroblasts concerning MF activation (Fig. 7A). At baseline, mLF-hT cells exhibited typical small fibroblast morphology and low amounts of the MF markers α-SMA, extradomain-A fibronectin (*70*), and Cdh11, all of which increased upon treatment with active TGF-β1 (Fig. 7A). Transient knockdown with two Cdh-specific targeting small interfering RNA (siRNAs) (siA and siB) either alone or in combination resulted in substantially lower Cdh11 protein amounts (fivefold reduction) compared with cells transfected with nontargeting siRNA, mock-transfected, or nontransfected (Fig. 7B). Cdh11 knockdown strongly reduced the formation of homocellular junctions between mLF-hT cells that were pretreated with TGF-β1 compared to cells treated with the control siRNA after TGF-β1 pretreatment (Fig. 7C). Likewise, M2 macrophage spreading on monolayers of Cdh11-knockdown MFs was significantly reduced compared to MFs transfected with the control siRNA (Fig. 7D), confirming the earlier results from experiments with Cdh11 function–blocking antibodies (Fig. 5, E to G). Knockdown of Cdh11 did not affect the abundance of α-SMA, latent TGF-β1, Cdh2, or β-catenin (Fig. 7B) or the expression of transcripts encoding α-SMA, Cdh11, Cdh2, or any of the integrin subunits previously shown to be involved in latent TGF-β activation (Fig. 7E).

Cdh11 establishes proximity for macrophages and MFs that enhances local amounts of active TGF-β1

Our results obtained in monocultures show that engagement of Cdh11 alone was neither sufficient to induce TGF-β activation by macrophages nor required to maintain MF activation. Thus, we propose that the primary physiological function of Cdh11 is to establish MF-macrophage coupling for close paracrine signaling. Macrophages are well-known suppliers of latent TGF-β in fibrotic conditions, whereas activation of latent TGF-β1 is most often performed locally by the recipient cells—fibroblasts—through integrin engagement with the latent TGF-β complex (*71*, *72*). To test whether close proximity of macrophages is required for latent TGF-β activation by MFs, we established transwell proximity coculture assays. For measuring active TGF-β signaling in Cdh11-blocking experiments, proximity assays were more suitable than direct macrophage-MF coculture because a substantial portion of macrophages detached from MF monolayers upon Cdh11 inhibition (Fig. 4, A and E). M2 macrophages grown on the bottom side of culture insert filter membranes were superimposed over MFs grown on stacks of coverslip supports of differing thickness (Fig. 8A). This setup allowed the measurement of active TGF-β by probing for the phosphorylation of the TGF-β signaling effectors Smad2 and Smad3 (Smad2/3) exclusively in the MF population. Active TGF-β signaling in MFs was only detected at a gap of ≤100 μm between the M2 macrophages and MF substrates (Fig. 8A). TGFRII-Fc partly blocked phosphorylation of Smad2/3 at this distance (Fig. 8B). Considering cell heights of 25 to 50 μm (measured from confocal z-scans; Fig. 3C), M2 macrophages and MF thus needed to be closer than 50 μm or in direct contact to establish active TGF-β signaling in the heterocellular couple. Inhibition of Cdh11 using function-blocking antibodies in the 100-μm gap setup did not significantly reduce proximity-dependent active TGF-β signaling in the MF population (Fig. 8C). From these results, we conclude that Cdh11 junctions facilitate TGF-β presentation and activation in macrophage-MF pairs by maintaining proximity between the two cell types in a pathophysiological context. If this Cdh11 function is replaced with experimentally forcing macrophages and MFs into close proximity, then heterocellular junction formation becomes dispensable.

DISCUSSION

Macrophages and fibroblastic cells both produce CDH11 during normal tissue repair and in fibroproliferative diseases. We have previously shown that Cdh11 production is enhanced during fibroblast-to-MF activation (*20*) and now provide evidence that activation with IL-4 and IL-13 results in a similar increase in Cdh11 in cultured mouse macrophages. Because CDH11 can promote homotypic adhesion, we proposed a function role for heterocellular binding between macrophages and MFs through CDH11 junctions and investigated the functional consequences. We show that CDH11 is present between activated macrophages and MFs in fibrotic lung tissue from both humans and mice and promotes specific recognition and strong adhesion between these cell types in cell culture. These functions are instrumental in promoting proximity, which establishes intimate TGF-β signaling between latent TGF-β–producing macrophages and MFs that maintain their profibrotic phenotype in the presence of active TGF-β.

Roles of CDH11 in fibrosis and wound healing

CDH11 has been introduced as a marker for MF activation in cultured corneal, subcutaneous, and lung fibroblasts (*20*, *24*). A shift from Cdh2 to Cdh11 production during MF activation in rat cells has been shown to enable the segregation of Cdh11-positive MFs from α-SMA– and Cdh11-negative fibroblasts through the formation of homocellular aggregates (*20*). Using atomic force microscopy, we demonstrated that individual Cdh11 bonds are stronger than Cdh2 bonds (*60*) and that such strong junctions are important to mechanically coordinate the contractile activity of MF populations (*73*). Consequently, inhibition or knockdown of CDH11 reduces the contraction of collagen and fibrin gels populated with subcutaneous MFs (*20*), Dupuytren's MFs (*33*), or dermal fibroblasts (*74*), and reduces calcified nodule formation by aortic valve MF contraction (*31*). Others have proposed that CDH11 also plays a direct role in transmitting cell force to the ECM by binding to fibronectin at sites of focal adhesions together with syndecan-4 (*75*). However, we did not observe an effect of cadherin-antagonizing peptides on the contractile activity of isolated rat MFs grown on fibronectin-coated deformable silicone elastomers in our earlier work (*20*) or reduced attachment of mouse MFs to culture dishes in the presence of Cdh11-blocking antibodies in the present study. In conjunction with transmitting and perceiving high intercellular tension, CDH11 is also involved in regulating MF profibrotic functions. Functional inhibition of CDH11 with antibodies or peptides resulted in reduced

Downloaded from http://stke.sciencemag.org/ on January 15, 2019

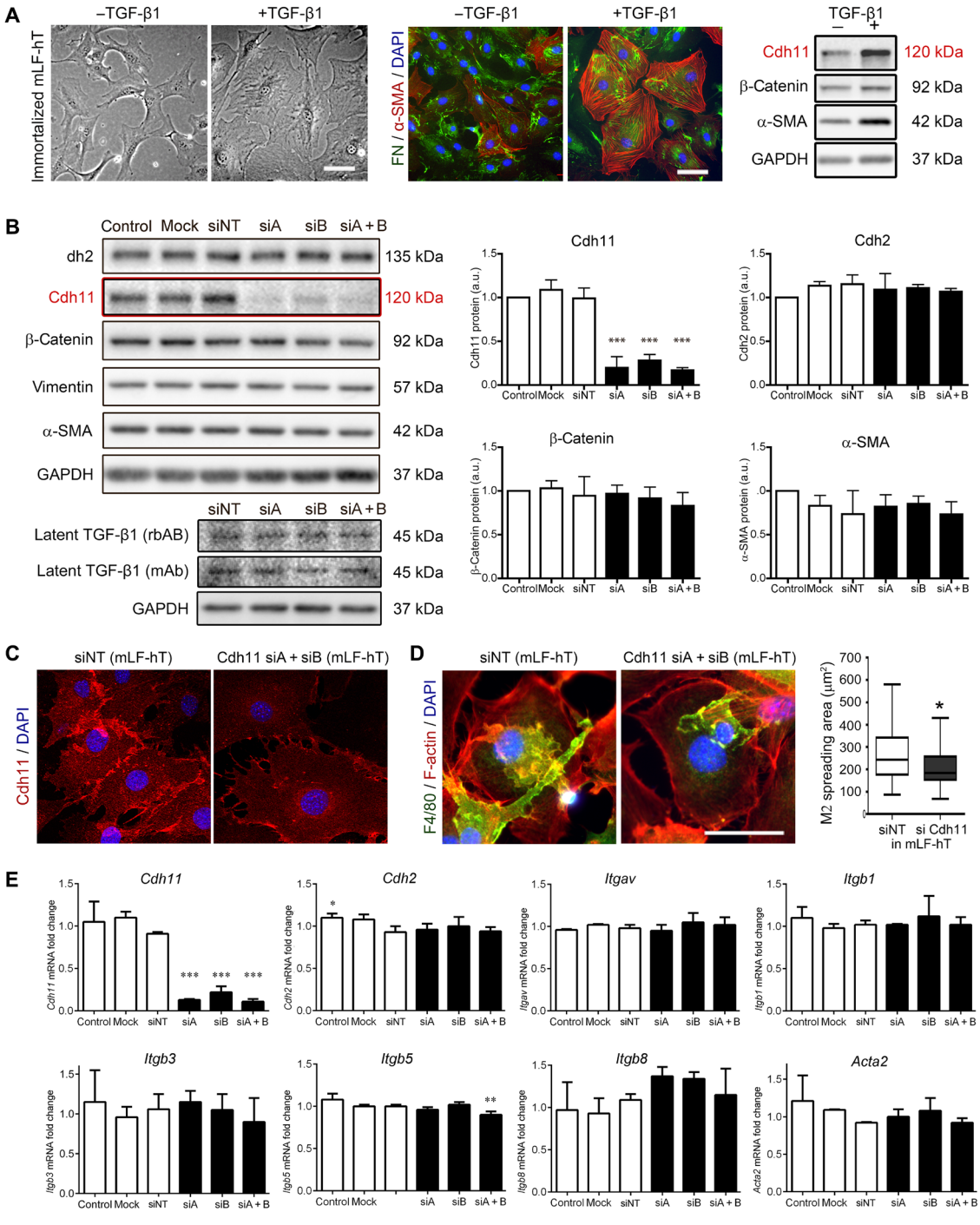

Fig. 7. Knockdown of Cdh11 in immortalized mouse lung MFs. (**A**) hTERT-immortalized mLFs (mLF-hT cells) cultured in the absence or presence of TGF-β1were examined by phase-contrast microscopy; by immunofluorescence staining for the MF markers α-SMA, extradomain-A fibronectin (FN), and nuclei (DAPI); and by Western blotting for Cdh11, β-catenin, and α-SMA. GAPDH is a loading control. Representative data from $n = 3$ independent batches of mLF-hT cells. (**B**) Western blot and quantification of Cdh2, Cdh11, β-catenin, vimentin, α-SMA, and TGF-β1 in mLF-hT cells that were transfected with two different Cdh11-targeting siRNAs alone (siA and siB), both CDH11-targeting siRNAs together (siA + B), a nontargeting siRNA (siNT), or no siRNA (mock). Cells that were not subjected to the transfection protocol were included as negative controls (control). Protein quantifications were first normalized to GAPDH and then to nontransfected controls. (**C**) Representative immunofluorescence images showing Cdh11 at junctions between mLF-hT cells that were pretreated with TGF-β1 before Cdh11 knockdown (Cdh11 siA + siB) or treatment with a nontargeting siRNA (siNT). (**D**) Representative immunofluorescence images showing the macrophage marker F4/80, F-actin, and nuclei (DAPI) in M2 macrophages plated on monolayers of mLF-hTs that were pretreated with TGF-β1 before Cdh11 knockdown (Cdh11 siA + siB) or transfection with the nontargeting siRNA. The fluorescence images were used to quantify the average spreading area of the macrophages. Graphs shows median, minimum, and maximum in box plots from $n = 3$ independent coculture experiments (*$P < 0.05$, two-tailed paired Student's t test). (**E**) Quantitative [qRT-PCR (quantitative reverse transcription polymerase chain reaction)] assessment of cell adhesion–related gene expression in TGF-β1–pretreated mLF-hTs upon Cdh11 knockdown and controls. Quantifications were first normalized to the average value of *G6pd*, *Gapdh*, and *Hmbs* and then to the siNT condition. All graphs except (D) show means ± SD from $n = 3$ independent transfection experiments (*$P < 0.05$ and ***$P < 0.001$, ANOVA with Tukey's multiple comparisons test).

amounts of ECM deposition in lung and skin fibroblast cultures (*27*, *29*, *74*). Cdh11 knockout or inhibition attenuated and partly reversed bleomycin-induced lung and skin fibrosis in the mouse and is associated with reduced collagen deposition (*27*, *29*). Whether CDH11 inhibition also affects the MF contractile phenotype (α-SMA organized into stress fibers) is less clear. Knockdown of CDH11 was shown to prevent the differentiation of fibroblast-like mesenchymal stem cells into α-SMA–positive smooth muscle cells in vitro and in vivo (*76*). Other studies either did not assess direct effects of Cdh11 knockdown or deficiency on α-SMA abundance (*29*, *31*, *74*) or, conversely, demonstrated

Downloaded from http://stke.sciencemag.org/ on January 15, 2019

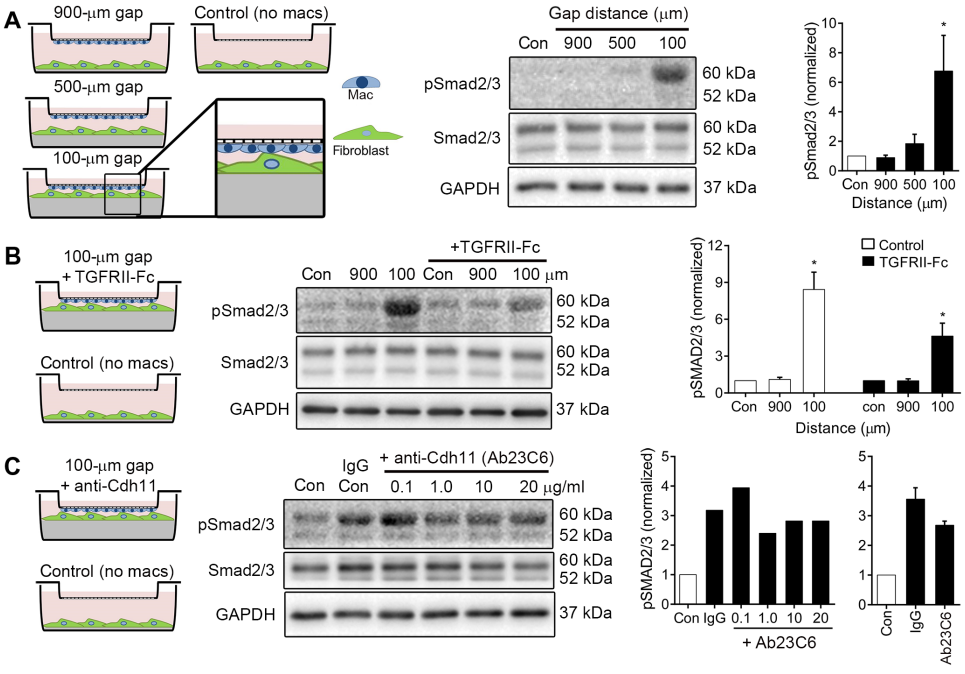

Fig. 8. Proximity dependence of macrophage-activated TGF-β1 signaling in fibroblasts. (**A**) A proximity culture system was used to vary the distance between fibroblasts and macrophages in coculture. Fibroblast monolayers were grown on culture substrates of different heights below M2 macrophages adhering to the underside of membrane Transwells. Empty Transwells without macrophages were used as a negative control (con). Effective gap distances were 900, 500, and 100 μm, not taking cell heights into account. TGF-β1 signaling in fibroblasts was assessed by immunoblotting cell lysates for total Smad2 and Smad3 (Smad2/3) and phosphorylated Smad2/3 (pSmad2/3). GAPDH is a loading control. Protein quantifications were first normalized to GAPDH and then to total Smad2/3 amounts. (**B** and **C**) The experiment was repeated at 900- and 100-μm gap distances in the presence of the TGF-β1 inhibitor TGFRII-Fc (B) or the Cdh11-blocking antibody 23C6 and control IgG (C). Graphs show means ± SD from $n = 3$ repeats (*$P \leq 0.05$, using ANOVA followed by a post hoc Tukey's multiple comparisons test).

an unexpected increase in α-SMA after Cdh11 knockdown (*32*). Our own data do not support a direct effect of transient Cdh11 knockdown on the abundance of protein or transcripts in monocultures of mLFs.

CDH11 mediates adhesion between activated macrophages and MFs

We identify a mechanism wherein CDH11 promotes specific binding between macrophages and MFs and thereby contributes to the activation and maintenance of the activated MF phenotype. Neoexpression of CDH11 in inflammatory cells (*29*) and alveolar macrophages (*27*) has previously been reported in skin and lung fibrosis, but the function of CDH11 in macrophages and possible binding to CDH11 on MFs remained elusive. Our data reveal the presence of CDH11 between CD68-positive macrophages and α-SMA–positive MFs in fibrotic mouse and human lung tissues. Our own tissue data and mining of array data from GEO datasets of mouse, rat, and human fibrotic lung seem to indicate that CDH11 is abundant during inflammation and the early stages of fibrosis. These datasets also suggest that the production and function of CDH11 in fibrosis is conserved between mouse and human. However, general differences that exist between human and rodent macrophage populations, and which macrophage phenotypes produce CDH11 in vivo, in particular in human, remain to be determined. Other studies observed induction of *Cdh11* mRNA after stimulating mouse alveolar lineage macrophages with LPS (*27*). In contrast, stimulation of mouse bone marrow–derived macrophages with IL-4 and IL-13 (profibrotic M2) in vitro achieved higher Cdh11 induction compared with LPS (proinflammatory M1) stimulation. These seemingly conflicting results confirm that the in vitro M1 and M2 classification has only limited relevance to the breadth of macrophage phenotypes in vivo. For instance, although we here defined IL-4– and IL-13–activated M2 macrophages as profibrotic in agreement with previous studies (*77*, *78*), recent work also demonstrates fibrosis-suppressing actions of M2 macrophages (*4*). Profibrotic or antifibrotic actions of presumably similar macrophage polarization states likely depend on the cellular context, including the activation state of fibroblastic cells sharing the same microenvironment.

Confocal and electron microscopy resolved Cdh11 junctions between IL-4– and IL-1–activated macrophages and MFs in cocultures. Functional assays demonstrated that (*1*) the presence of Cdh11 on both macrophages and MFs results in their specific recognition of one another in aggregation assays, (*2*) allows attachment and spreading of macrophages on MFs, and (*3*) mediates strong mechanical binding. Residual adhesion of macrophages to MFs remained after functional blocking or knockdown of Cdh11, suggesting that alternative but weaker adhesion mechanisms (perhaps Cdh2-mediated) between these cells also exist. One important direct outcome of Cdh11 binding is retention of macrophages near MFs, allowing persistent and close cell-cell communication. While our work was under review, the importance of physical cell-cell contacts to establish stable signaling "circuits" between fibroblasts and macrophages was demonstrated experimentally and with mathematical models (*79*). Macrophage-MF intimacy has been reported in various fibrotic organs and is suggested to promote fibrosis by locally regulating the activation state of fibroblastic cells (*36*, *80*–*84*). Consistent with this, we show that proximity or direct contact is essential for macrophages to induce fibroblast-to-MF activation in a TGF-β–dependent manner in cocultures. Macrophages are a predominant source of TGF-β in conditions of fibrosis (*80*, *85*), but there are conflicting data on the ability of macrophages to activate TGF-β. Seminal studies performed with antibodies specific to active TGF-β have shown that peritoneal macrophages produce active TGF-β when stimulated with LPS and interferon-γ (IFN-γ) in culture (*40*–*42*). In contrast, we were not able to detect substantial amounts of active TGF-β in cultured primary mouse bone marrow–derived macrophages. This finding is consistent with earlier studies that did not detect active TGF-β in macrophage-conditioned medium using the same TMLC reporter assay used in this study (*40*). Alveolar macrophages isolated from the lungs of Cdh11-deficient mice exhibit lower TGF-β amounts than cells from control mice when measured

Downloaded from http://stke.sciencemag.org/ on January 15, 2019

with enzyme-linked immunosorbent assay (*27*), and IL-4–stimulated Cdh11 knockout macrophages produce lower amounts of TGF-β compared to wild-type macrophages in culture (*29*). However, these studies did not discriminate between active and latent TGF-β, and whether TGF-β secretion is a direct consequence of knocking out Cdh11 cannot be concluded from these data. In vitro–polarized wild-type macrophages did not show any correlation between the amounts of Cdh11 and TGF-β in our study. For instance, LPS-stimulated M1 macrophage cultures contained high amounts of latent TGF-β but were virtually negative for Cdh11. However, all polarized macrophage types produced high amounts of latent TGF-β that became active and available upon Cdh11-mediated or experimentally forced direct contact between M2 macrophages and fibroblastic cells.

It has been suggested that CDH11 plays a role in regulating TGF-β1 expression in macrophages (*26*). However, our data do not support that Cdh11 enhances the production of TGF-β but rather enables Cdh11-positive macrophages to specifically deliver their latent TGF-β load to Cdh11-positive MFs for local activation. This idea is consistent with profibrotic TGF-β signaling being spatially restricted to the site of latent TGF-β activation. In their seminal studies, the Rifkin and d'Amore laboratories demonstrated conversion of latent into active TGF-β1 in heterocellular cocultures of smooth muscle and endothelial cells but not in the respective monocultures (*86*, *87*). Highly localized latent TGF-β1 activation by epithelial integrins was later identified as a predominant driving mechanism for lung fibrosis (*88*). Cell pulling on the latent TGF-β1 complex through αv integrins (*89*) has emerged as one of the predominant cellular mechanisms of TGF-β1 activation in fibrosis (*69*, *90*–*92*). A similar "TGF-β1 handshake" mechanism is also suggested to be used by regulatory T cells to control the activity of other T cells or tumor cells (*93*–*95*). It is conceivable that macrophages carry latent TGF-β in a plasma membrane–bound complex, such as leucine-rich repeat containing 32 (LRRC32) on the surface of regulatory T cells (*96*–*99*) and platelets (*100*) or LRRC33 on the surface of microglia (*101*). The mode of latent TGF-β delivery or presentation by macrophages to fibroblasts and the activation mechanisms are under current investigation in our laboratory. To this end, we cannot exclude that MFs secrete short-ranging factors that stimulate macrophages to activate TGF-β1 themselves or that direct contact with macrophages stimulates MFs to contract and release active TGF-β1 from their own ECM (*69*). TGF-β is also not the only profibrotic factor secreted by macrophages. Although we were able to block macrophage proximity–induced activation of MFs with TGF-β1 antagonists, residual activation remained insensitive to TGF-β1 inhibition. This can be explained by incomplete accessibility of active TGF-β1 to the blocking compound in the macrophage-MF space or the contribution of other macrophage-secreted factors, such as IL-1 or platelet-derived growth factor (*36*, *79*).

Possible direct signaling effects of CDH11-CDH11 junction formation

In addition to establishing proximity for TGF-β1 delivery and activation between macrophages and MFs, it is possible that CDH11 engagement directly triggers profibrotic signaling. Growth on CDH11:Fc-coated surfaces has been shown to induce Smad2 phosphorylation and transcription of ECM genes in cultured fibroblasts, but the mechanistic link between CDH11 engagement and Smad phosphorylation remained elusive (*74*). The role of TGF-β1 is unclear in this signaling process because Smad2 phosphorylation upon CDH11 binding is blocked by inhibiting the TGF-β receptor but not with TGF-β1–blocking antibodies, and TGF-β activation was not assessed in that study (*74*). One possibility is that growth on CDH11 substrates allows development of higher intracellular tension than growth on CDH2-coated substrates (*60*), which were used as control in that study (*74*). Mechanical stress is pivotal for MF activation (*102*, *103*). Growth on CDH11 substrates did not promote α-SMA production and MF activation in our hands. Although direct effects of macrophage Cdh11 binding on MF activation and enhanced Smad signaling cannot be excluded in our experiments, they seem to play a minor role in the coculture context. First, our experiments were performed at cell confluency, allowing MFs to form CDH11-positive junctions with one other. Second, inhibition of Cdh11 with function-blocking antibodies did not alter macrophage-induced Smad phosphorylation in MFs in forced proximity assays. Third, growth on CDH11:Fc surfaces did not elicit a TGF-β1 activation response in either macrophages or fibroblasts. Last, knockdown of Cdh11 in MFs did not change total TGF-β1 abundance or the transcript or protein abundance of α-SMA, a direct downstream target of Smad-mediated TGF-β signaling.

CONCLUSION

Recent studies have shown that CDH11 deficiency or inhibition reduces experimentally induced organ fibrosis and TGF-β signaling in fibroblastic cells, but the molecular function of CDH11 remained elusive (*27*, *29*). We provide evidence for a mechanism wherein CDH11 physically couples activated macrophages and MFs and thereby establishes a niche of active TGF-β. In this scenario, even low numbers of macrophages could effectively promote fibrosis by prolonging MF activation. After acute injury, lung macrophages are among the first cellular responders to enter the provisional wound ECM, which is initially lacking fibroblastic cells. It is conceivable that these early-arriving macrophages produce TGF-β, which is either activated in the aggressive milieu of the wound or stored in the ECM. While early macrophages are being cleared, fibroblasts migrate into the wound site and, with increasing strain in the ECM, are able to access and gradually deplete latent TGF-β stores (*104*). It is tempting to speculate that dysregulated timing of macrophage clearance and MF activation results in the retention of CDH11-positive macrophages by CDH11-positive MFs in pathology. This engagement would facilitate TGF-β1 exchange and persistence of both cell types. CDH11-dependent signaling is bidirectional, and the presence of CDH11 promotes IL-33 production in fibroblastic synoviocytes. Synoviocyte-secreted IL-33, in turn, controls proinflammatory profiles in macrophages in the context of adipose tissue inflammation and diabetes (*105*). Hence, interfering with CDH11 accumulation or function, or both, in inflamed and fibrotic tissues would target inflammatory signaling and enable separation of both cell types to eventually terminate profibrotic communication.

MATERIALS AND METHODS

Human lung tissue

Human lung tissue was obtained from the Department of Pathology (McMaster University, ON, Canada) from patients diagnosed with IPF. Research on archived human specimens was approved by the Hamilton Integrated Research Ethics Board under protocol no. 11-3559.

Downloaded from http://stke.sciencemag.org/ on January 15, 2019

Samples were arranged as a tissue array containing formalin-fixed and paraffin-embedded 5-μm-thick specimens (0.4 mm^2 per tissue core biopsy) including four replicate cores of IPF fibrotic regions and four replicate cores of patient-matched non-fibrotic (but inflamed) lung tissues (n = 25 patients with IPF). Additional non-fibrotic control tissues were obtained from archived tissue samples from patients with lung cancer resections from tumor-free tissues (n = 5). All samples included in the study were examined by molecular pathologists and were selected on the basis of a typical histological presentation of usual interstitial pneumonia or by a normal non-fibrotic presentation for the control samples.

Animal experiments

Wild-type male C57BL/6J mice at 8 to 12 weeks of age were used according to the current guidelines by the American Thoracic Society (*106*). Experimental pulmonary fibrosis was induced using intratracheal intubation of bleomycin at 0.04 U per mouse in a volume of 50-μl sterile saline (Hospira Healthcare Corporation, NDC 61703-332-18); control animals received only saline (*107*). Animal groups were euthanized after 7 or 21 days. To collect lung tissue, the lungs were cannulated, excised, and washed with PBS. For histological analysis, the left lung was removed and inflated to 30 centimeters of water (cmH_2O) for 3 to 5 min in 10% formalin solution and fixed for 48 to 72 hours before paraffin embedding. For Western blotting, lung tissues were snap frozen in liquid nitrogen, crushed, and then homogenized in radioimmunoprecipitation assay buffer with protease inhibitors [1% nonionic, nondenaturing detergent (IGEPAL CA-630), 0.5% Na-deoxycholate, 0.1% SDS and 1 mM Na-orthovanadate, aprotinin (5 μg/ml), 1 mM phenylmethylsulphonyl fluoride, and 1 mM dithiothreitol in PBS].

To collect alveolar macrophages, BAL was performed on CO_2-euthanized 8-week-old, wild-type C57BL/6J male mice (n = 12 bleomycin-challenged and n = 13 PBS control). The trachea was cannulated, and lungs were flushed four times with 800-μl ice-cold 1 mM EDTA-PBS, followed by washing of the collected cells with 200-μl ice-cold 1 mM EDTA-PBS. Cells were counted in the presence of Trypan blue stain (viability > 95%) and resuspended in Ham's F12/Dulbecco's minimum essential medium (DMEM) supplemented with 10% fetal bovine serum (FBS), 1% penicillin/streptomycin (P/S), and 3% L-glutamine. Cells derived from two to five mice per condition were pooled to obtain sufficient cell numbers for experimental analysis (110,000 cells per pooling). To collect tissue-resident macrophages, the BAL-flushed mouse lungs were dissected into lobes, rinsed with PBS, minced, and digested using a cocktail of RPMI 1640 medium (WISENT), containing liberase [collagenase (13 U/ml) and total collagenase (2.5 mg/ml)] and deoxyribonuclease I (0.4 mg/ml) both (Roche) for 30 min at 37°C. Digestion was terminated with PBS containing 100 mM EDTA at equal volume, and the digest was passed through a 70-μm mesh cell strainer (BD Biosciences). Cells were collected from the strainer by washing once with RPMI, followed by centrifugation at 1500 rpm for 5 min at 4°C and resuspension of the pellet in red blood cell lysis buffer (eBioscience) for 5 min at room temperature. Last, the reaction was diluted three times with Hanks' balanced salt solution.

Cell culture

Fibroblasts were explanted from the lungs of C57BL/6 mice and subcultured for up to five passages in DMEM, supplemented with 10% FBS and 1% P/S. MFs were generated by 4-day treatment with TGF-β1 (2 ng/ml) in the passage preceding the experiment (fig. S1). Fibroblasts were generated by suppressing MF activation with the competitive TGF-β1 receptor inhibitor SB431542 (50 μM) and growth on lung-soft (5-kPa elastic modulus) silicone substrates (*108*) (ExCellness Biotech SA), coated with gelatin (2 $\mu g/cm^2$) (Sigma-Aldrich). To obtain primary macrophages, femur and tibia of C57BL/6 mice were dissected, and bone marrow was flushed using macrophage base medium (45% DMEM, 45% Ham's F12, 3% L-glutamine at 200 mM, 10% FBS, and 1% P/S) (WISENT) supplemented with M-CSF (20 ng/ml) (Life Technologies), followed by 7-day culture in the same medium (M0 macrophages). Mature macrophages were polarized by adding LPS (100 ng/ml) (Sigma-Aldrich) to generate M1 macrophages or IL-4 (10 ng/ml) (PeproTech) plus IL-13 (10 ng/ml) (Bio Basic Inc.) to generate M2 macrophages for additional 4 days. Cocultures of macrophages with fibroblastic cells were performed in macrophage base medium. For one experimental series, macrophages were cultured on cell culture surfaces coated with recombinant CDH11:Fc, which has been characterized for physiological function in previous cell- and single molecule–binding studies (*21*, *34*, *60*, *74*, *109*).

To generate immortal mLFs (*mLF-hT* cells), Gryphon retroviral packaging cells (Allele Biotechnology) were transfected with a plasmid containing hTERT, pBABE-hygro-hTERT (Addgene) (*110*), using FuGENE HD (Roche). The retrovirus particle–containing supernatant was harvested at 72 hours after transfection and separated from cell debris by centrifugation. Primary mLFs at passage P3 were infected with hTERT retrovirus particles in the presence of polybrene (1 μg/ml) (Sigma). Three hours after infection, the medium was changed, and transformed cells were selected using hygromycin B (300 μg/ml) (Bio Basic) after another 48 hours. Resistant cells were expanded, and the growth rate was monitored and compared to primary mLFs. Primary fibroblasts entered senescence at passage P7, whereas transfected mLF-hT cells continued proliferating beyond passage P40 (doubling time of 28 hours).

Immortalized mLF-hT cells were used to knock down Cdh11. Briefly, cells were trypsinized, washed with PBS, and resuspended in electroporation buffer [(137 mM NaCl, 11.2 mM Na_2HPO_4/NaH_2PO_4, and 5 mM KCl (pH 7.4)] at 200,000 cells per 100 μl. For siRNA transfection, electroporation was performed (Neon, Invitrogen) in 100-μl electroporation solution containing 50 μM ON-TARGETplus nontargeting siRNA no. 2 (siNT) (D-001810-02-05, Dharmacon), 50 μM mouse *Cdh11*-targeting custom siRNA (siA) (Thermo Scientific, target sequence: GUAAGAGACAACAGAGAUAUU), or 50 μM ON-TARGETplus mouse *Cdh11*-targeting siRNA (siB) [SMARTpool, L-053105-00-0005; Thermo Scientific, target sequences: CAAUUGAUCGUCAUACUGA, GGUCAUCGUUGUGCUGUUU, AGAUAACACUGCAGGAGUA, GCUUAUAGCUUGAAGAUAG, or combination of si*Cdh11* (siA + B)]. Electroporation was performed with one pulse at 1350 V for 30 ms, the transfected cells were used after 48 hours.

Cell contractility was assessed using deformable silicone substrates as previously described (*102*). Briefly, polydimethylsiloxane substrates with a Young's modulus of 5 kPa were coated with fibronectin (10 μg/ml) for sparse fibroblast cultures. Wrinkle formation on substrates, indicating cell contraction, was observed after 24 hours in culture. Live phase-contrast images were acquired with an inverted microscope (Axiovert135, Carl Zeiss; 40× objective) and analyzed using ImageJ customized macros [U.S. National Institutes of Health (NIH), Bethesda, MA, USA; http://imagej.nih.gov/ij/; 1997–2013] by thresholding for phase-bright wrinkles and analyzing

Downloaded from http://stke.sciencemag.org/ on January 15, 2019

the surface area covered by identified particles in the resulting binary images. Relative contraction was expressed as image area covered by wrinkles normalized to cell numbers (*65*).

Active TGF-β measurements

Active TGF-β was quantified using TMLCs, which produce luciferase under the control of the PAI-1 (plasminogen activator inhibitor–1) promoter in response to TGF-β (fig. S3B) (*111*). Coculture experiments were performed by seeding TMLCs directly with macrophages, fibroblasts, or both macrophages and fibroblasts for the indicated times. TMLCs were lysed, and luminescence was quantified with a luciferase assay kit (Promega) and luminometer (Centro LB, Berthold Technologies). To assess TGF-β amounts in culture supernatants, TMLCs (60,000 cells/cm^2) were adhered for 4 hours before being subjected for 24 hours to conditioned media, native (active TGF-β) or heat activated for 10 min at 80°C (total TGF-β), respectively. All results were corrected for TMLC baseline luciferase production in the absence of TGF-β, and active TGF-β was normalized to total TGF-β1. TGF-β concentrations were determined from standard curves performed with known concentrations of active TGF-β1 (fig. S3C).

Immunofluorescence microscopy, flow cytometry, cytokine arrays, and Western blotting

For immunohistochemistry of lung tissue, paraffin sections were deparaffinized in xylene and rehydrated, followed by staining as described earlier (*107*, *112*). Briefly, citric acid buffer (pH 6) incubation for 15 min at 95°C was used as antigen retrieval followed by endogenous peroxidase inactivation using 3,3′-diaminobenzidine chromogen detection. For immunofluorescence, tissue antigens were retrieved by boiling in tris buffer [10 mM tris, 1 mM EDTA (pH 9), and 0.05% Tween 20] at 95° to 100°C for 20 min. After cooling, sections were rinsed in tris-buffered saline (TBS) with 0.025% Triton X-100, blocked with 10% goat serum, and 1% bovine serum albumin (BSA) in TBS for 1 hour, and then stained with primary and secondary antibodies in 1% BSA in TBS. Cultured cells were fixed in 3% paraformaldehyde (PFA) and permeabilized with 0.2% Triton X-100. Samples were incubated with primary antibodies directed against CDH11 [23C6 monoclanal antibody (mAb), a gift from M. Brenner, Harvard Medical School; mIgG1, Thermo Fisher Scientific, clone 5B245, catalog no. 32-170], α-SMA (mIgG2a, a gift from G. Gabbiani, University of Geneva), F4/80 (only for mouse cells and tissues: rat IgG2b, BioLegend, catalog no. 122602), β-catenin [rabbit (rb), Millipore, catalog no. AB19022(CH)], CD206 (rb, Abcam, catalog no. AB64693), CD68 (for cells: rat IgG2a, Abcam, clone FA-11, catalog no. ab53444; for tissues: msIgG3, Dako, clone PG-M1, catalog no. M0876), and TGF-β (Cell Signaling Technology, clone 56E4 mAb, catalog no. 3709 and rbAb, catalog no. 3711). Primary antibodies were followed by incubation with secondary antibodies goat anti-mouse IgG Alexa Fluor 568 (Life Technologies, catalog no. A-11004), goat anti-mouse IgG1 fluorescein isothiocyanate (FITC) (SouthernBiotech, catalog no. 1070-02), goat anti-mouse IgG2a tetramethyl rhodamine isothiocyanate (TRITC) (SouthernBiotech, catalog no. 1080-03), goat anti-mouse IgG3 Alexa Fluor 488 (Invitrogen, catalog no. A-21151), and goat anti-rabbit–TRITC and –FITC (Sigma-Aldrich, F9887). Phalloidin–Alexa Flour 488 (Life Technologies) was used to stain F-actin, and DAPI dihydrochloride (Sigma-Aldrich, D9542) was used to stain DNA.

Confocal fluorescence microscopy images were acquired with a Leica True Confocal System SP8 with HC PL APO (plan-field flatness correction, apochromatic) CS2 63×/1.40 oil objective or an Axio Imager upright microscope equipped with an AxioCam HRm camera, Apotome.2 structured illumination, and ZEN software (ZEISS). Plan Apochromat objectives were used [ZEISS, 40×, 1.2 numerical aperture (NA) and ZEISS, 63×, 1.4 NA, oil differential interference contrast] in addition to a Fluar objective (ZEISS, 20×, 0.75 NA). Figures were assembled in Adobe Photoshop CS5 (Adobe Systems). For image analysis of histological sections, stained tissue slides were scanned (ZEISS Axio Scan.Z1 slide scanner with Plan Apochromat 20× objective, ZEISS) and analyzed using IQ4-HALO pattern recognition software (PerkinElmer). On the basis of α-SMA signal (MF) quantification after subtraction of desmin signal (smooth muscle), five samples from IPF patients with the highest MF score were selected for detailed analysis.

Immunoblotting was performed according to standard procedures. Blots were probed with primary antibodies used in immunofluorescence in addition to CDH11 (rb, Cell Signaling Technology, clone P707, catalog no. 4442), Cdh2 (mIgG1, Zymed, catalog no. 610920), α-catenin (rb, Zymed, catalog no. 71–1200), β-catenin (rb, Millipore), α-tubulin (mIgG1, Sigma-Aldrich, DM1A, catalog no. T9026), pSMAD2/3 (rb, Cell Signaling Technology, clone D27F4, catalog no. 8828S, total SMAD2/3 (rb, Cell Signaling Technology, clone D7G7, catalog no. 8685), GAPDH (mIgG1, Chemicon, catalog no. MAB374), CD68 (rat IgG2a, Abcam), CD206 (rb, Abcam), iNOS (rb, Abcam, catalog no. ab15323), Arg-1 (mIgG1, BD, catalog no. 610709), and vimentin (mIgG1, Dako, M0725). Horseradish peroxidase–conjugated secondary goat anti-mouse (catalog no. M32507) and goat anti-rabbit (catalog no. 656120) antibodies (Invitrogen) were used for chemiluminescence detection (Invitrogen). Images were acquired using the LI-COR system, and densitometry analysis was performed with Image Studio software. For flow cytometry of subcultured macrophages, the cells were gently detached using Accutase (StemPro, Life Technologies), Fc receptors were blocked using TruStain FcX blocker (anti-mouse CD16/CD32, clone 93, BioLegend, catalog no. 101320), and cell viability was determined using fixable viability dye eFluor 506 (eBioscience). Cells were live labeled with fluorochrome-conjugated primary antibody mix containing F4/80–Brilliant Violet (ratIgG2a, κ, BioLegend, catalog no. 123131), CD80-AF488 (msIgG1, κ, BioLegend, clone 2D10, catalog no. 305214), and CD206-PE (R-Phycoerythrin) (ratIgG2a, κ, BioLegend, catalog no. 141705). Macrophages were then fixed in PFA, passed through a cell strainer, run through CytoFLEX (Beckman Coulter), and analyzed using FlowJo software (Treestar).

For FACS of macrophages from mouse lung tissue digests, cells were resuspended in PBS containing 4% FBS and 25 mM Hepes and labeled with fluorochrome-conjugated primary antibody mix containing fixable viability dye eFluor 506, CD45-PE/Cy7 (rat IgG2b, κ, BioLegend, clone 30-F11, catalog no. 103114), CD64-PE (mouse IgG1κ, BioLegend, clone X54-5/7.1, catalog no. 139303). Cells were then passed through a 35-μm cell strainer cap. Viable CD45/CD64 double-positive cells were sorted into FBS using a FACSAria III and FACSDiva 8.0 software (BD Biosciences). Immediately after the sort, mRNA was extracted as described above. All antibodies and reagents for flow cytometry were obtained from BioLegend.

To quantify cytokine production, macrophages were polarized as described above and subsequently cultured in macrophage base medium for 2 days. Conditioned culture supernatants were analyzed using a mouse cytokine array, comprising BLC (B lymphocyte chemoattractant), C5/C5a (fragment of complementary protein C5),

Downloaded from http://stke.sciencemag.org/ on January 15, 2019

G-CSF (granulocyte CSF), GM-CSF (granulocyte-macrophage CSF), I-309, eotaxin, sICAM-1 (soluble intercellular adhesion molecule–1), IFN-γ, IL-1α, IL-1β, IL-1ra, IL-2, IL-3, IL-4, IL-5, IL-6, IL-7, IL-10, IL-13, IL-12p70, IL-16, IL-17, IL-23, IL-27, IP-10 (IFN-γ–inducible protein 10), I-TAC (interferon-inducible T cell alpha chemoattractant), KC (keratinocyte chemoattractant), M-CSF, JE/MCP-1 (monocyte chemoattractant protein–1), MCP-5 (monocyte chemoattractant protein–5), MIG (monokine induced by IFN-γ), MIP-1α (macrophage inflammatory protein–1α), MIP-1β, MIP-2, RANTES, SDF-1 (stromal cell–derived factor–1), TARC (thymus and activation regulated chemokine), TIMP-1 (tissue inhibitor of matrix metalloproteinases–1), TNF-α (tumor necrosis factor–α), and TREM-1 (triggering receptor expressed on myeloid cells–1) (Panel A, Proteome Profiler, R&D Systems), according to the manufacturer's specifications. Cytokine binding to array membranes was detected by chemiluminescence using a digital system (Odyssey, LI-COR). Cytokine presence was determined by measuring the average luminescence intensity (pixel density) for each antibody spot for three independent experiments.

Scanning, transmission, and immunoelectron microscopy

For scanning electron microscopy, macrophages were grown on 10-mm glass coverslips, fixed with 2% glutaraldehyde in 0.1 M sodium cacodylate buffer (pH 7.3) for 2 hours, followed by 0.1 M sodium cacodylate buffer with 0.2 M sucrose (pH 7.3) for 20 min. Samples were dehydrated with ethanol in 10% increments from 50 to 100% for 20 min each and subsequently critical point dried (CPD 030, BAL-TEC, Balzers). Samples were mounted and gold sputtered (Desk II sputter coater, Denton), and images were taken with a XL-30 scanning electron microscope (Philips/FEI) at a tilt angle of 45°. For transmission electron microscopy, macrophages were grown for 24 hours on top of lung MF monolayers on a transwell insert with 0.4-μm pore size (Corning). Cells were fixed in 2% glutaraldehyde, 0.1 M sodium cacodylate buffer (pH 7.3) for 2 hours at room temperature. Samples were rinsed in 0.1 M sodium cacodylate buffer with 0.2 M sucrose (pH 7.3) followed by 1% osmium tetroxide post-fixation, dehydrated, and embedded in resin (Quetol-Spurr, Electron Microscopy Sciences). Ultrathin 90-nm sections were contrasted using uranyl acetate and lead citrate and examined using a transmission electron microscope (Tecnai 20, FEI, Eindhoven, The Netherlands) equipped with a digital camera (Gatan Orius, Gatan). For immunoelectron microscopy, culture membrane cocultures were fixed in 4% PFA/2.5% sucrose, immersed in 2.3 M sucrose, and frozen in liquid nitrogen, and 70-nm ultrathin sections were cut with a cryo-ultramicrotome (EM UC7, Leica). Sections were then incubated in 0.1% glycine in PBS followed by incubation in 1% BSA in PBS. Primary antibody directed against CDH11 (clone 23C6, 23 μg/ml) (*34*) was followed by secondary goat anti-mouse IgG (Jackson ImmunoResearch Europe Ltd., catalog no. 115-005-003) and incubation with Protein A–gold conjugates (10 nm). Sections were embedded in methylcellulose and examined in a Tecnai Spirit transmission electron microscope (FEI) equipped with a digital camera (QUEMESA, EMSIS GmbH).

Heterocellular adhesion and coculture assays

To assess direct cell-cell attachment, fibroblasts and MFs were grown for 4 days to a confluent monolayer and macrophages (ratio of 5:1 to fibroblasts) were added for 3 hours. After jet washing, remaining cells were fixed and stained for α-SMA (MFs), F4/80 (macrophages), and DAPI (nuclei), and 10 images were taken per condition. The number of adherent macrophages was determined by manually counting F4/80-positive cells, and macrophage area was calculated from the F4/80 signal; tracing macrophage cell edges was done with the freehand selection tool in ImageJ (NIH). To assess heterocellular aggregation, macrophages were mixed 1:1 with fibroblastic cells in microreaction tubes and rotated at 2 rpm in an incubator for 2 hours. Resulting aggregates were then plated and allowed to adhere for 3 hours before being fixed and stained for β-catenin (membrane and junctions), F4/80, α-SMA, and DAPI. At least 10 images were taken per condition, and the number of aggregates (≥2 contacting cells) was quantified per image field. The number of macrophages per aggregate was determined by counting F4/80-positive cells and related to the number of fibroblastic cells in the same aggregate (macrophages per fibroblasts). To assess macrophage attachment strength to fibroblasts or MFs, fibroblastic cells were cultured in the channels of parallel plate flow chambers (μ-Slide VI 0.4; ibidi) to form confluent monolayers. Macrophages were then seeded onto the monolayers (5:1 ratio) and allowed to adhere for 15 min before fluid flow was applied using a syringe pump (NE-1000, New Era Pump Systems). After removing non-attached and weakly attached macrophages with gentle fluid shear stress (1.1 N/m^2), shear stress was gradually increased to 5.5 N/m^2 in 30-s steps. For Cdh11 function blocking, we preincubated macrophage and MF monolayers for 1 hour with CDH11 antibodies 23C6 and 13C2 (*34*) or IgG controls at 0.05 μg/ml. Cadherin binding was nonspecifically inhibited with 2 mM EGTA in cell adhesion tests. Experiments were performed on an environmentally controlled microscope stage (Axiovert 135, ZEISS), and image sequences were acquired at one frame per minute using a phase-contrast objective (10×). The number of phase-bright macrophages remaining attached at the end of each flow rate step was quantified from the recorded movies with ImageJ (NIH) using customized macros.

To discriminate between paracrine signaling and direct contact between macrophages and fibroblasts, we custom designed 35-mm-diameter cell culture dishes containing two separate wells of 1 cm^2 that allowed cells to share the same culture medium. For physical separation, each cell type was cultured in one well; for direct contact, the equivalent cell number was used to seed macrophages in a ratio of 5:1 on top of MF monolayers in one well only. To systematically control proximity between macrophages and MFs, custom-produced polycarbonate cylindrical spacers were used to fit 24-well culture plates (d = 12 mm; h = 300 and 700 μm). Fibroblast monolayers were cultured overnight on gelatin (2 $\mu g/cm^2$)–coated 12-mm coverslips (h = 100 μm; Thermo Fisher Scientific), placed on top of the spacers. M2 macrophages were seeded onto the bottom of 6.5-mm polyester membrane Transwells (0.4-μm membrane pore size) (Corning) for 45 min to allow attachment and then grown upside down in macrophage polarization medium. For proximity cocultures, M2 macrophage–containing Transwells were inserted over the fibroblast monolayers, cultured in macrophage base medium, and cocultured at distances of 900, 500, and 100 μm (not counting cell heights) for 4 days.

Data mining and statistical analysis

All experiments were performed in at least three biological replicates. Quantitative data are presented as means ± SD. We assessed differences between groups with an ANOVA followed by a post hoc Tukey's multiple comparisons test and Dunnett's multiple comparisons test with significance levels set at $^*P = 0.05$ and $^{**}P = 0.01$. For experiments comparing two groups, we performed a two-tailed paired Student's t test. Differences were considered statistically significant and indicated with $^*P \leq 0.05$, $^{**}P \leq 0.01$, and $^{***}P \leq 0.005$. The GEO database

Downloaded from http://stke.sciencemag.org/ on January 15, 2019

was consulted to extract CDH11 mRNA expression values for human lung tissue (GEO accession numbers GSE24206 and GSE47460) and Cdh11 for rodent lung tissue (GEO accession numbers GSE42301 and GSE48455). For GSE47460 analysis, only fibrotic tissue from lungs with a forced vital capacity, an indicator of restriction by fibrosis, of <80% were considered. Mann-Whitney *U* test or Kruskal-Wallis test followed by Dunn's multiple comparisons test was used for not normally distributed variables, and two-tailed unpaired *t* test or one-way ANOVA followed by Dunnett's multiple comparisons test was used for normally distributed variables using GraphPad Prism version 6.00 for Windows (GraphPad Software, www.graphpad.com).

Quantitative reverse transcription PCR

Total mRNA was extracted using PureLink Mini RNA kit or PureLink Microscale RNA kit (both Invitrogen) according to the manufacturer's instructions. RNA (500 ng for *Cdh11* siRNA experiments and 50 ng for bleomycin-exposed macrophage experiments) was reverse transcribed with SuperScript VILO cDNA synthesis kit (Invitrogen). PCR amplification was performed in triplicate with RT^2 SYBR Green ROX reference dye (QIAGEN) by using StepOnePlus Real-Time PCR System (Applied Biosystems) at 95°C for 10 min, 40 cycles at 95°C for 15 s and at 59°C for 60 s, followed by the melt curve. Relative gene expressions were calculated by using mouse *Gapdh*, *Hmbs*, and *G6pd* as reference genes, as published elsewhere (*113*). For primers and annealing temperatures, see table S1.

Study approval

All animal work were conducted under the guidelines of the Canadian Council on Animal Care and approved by the Animal Research Ethics Board of McMaster University under protocol no. 12.02.06. All procedures pertaining to human tissue were approved by the Hamilton Integrated Research Ethics Board under protocol no.11-3559.

SUPPLEMENTARY MATERIALS

www.sciencesignaling.org/cgi/content/full/12/564/eaao3469/DC1
Fig. S1. Primary mLF cultures.
Fig. S2. Primary mouse macrophage cultures.
Fig. S3. Active TGF-β1 measurement using TMLC cultures.
Table S1. Primer list.

REFERENCES AND NOTES

1. B. Hinz, Myofibroblasts. *Exp. Eye Res.* **142**, 56–70 (2016).
2. J. S. Duffield, M. Lupher, V. J. Thannickal, T. A. Wynn, Host responses in tissue repair and fibrosis. *Annu. Rev. Pathol.* **8**, 241–276 (2013).
3. M. Walraven, B. Hinz, Therapeutic approaches to control tissue repair and fibrosis: Extracellular matrix as a game changer. *Matrix Biol.* **71–72**, 205–224 (2018).
4. T. A. Wynn, T. R. Ramalingam, Mechanisms of fibrosis: Therapeutic translation for fibrotic disease. *Nat. Med.* **18**, 1028–1040 (2012).
5. T. J. Gross, G. W. Hunninghake, Idiopathic pulmonary fibrosis. *N. Engl. J. Med.* **345**, 517–525 (2001).
6. T. A. Wynn, Integrating mechanisms of pulmonary fibrosis. *J. Exp. Med.* **208**, 1339–1350 (2011).
7. A. T. Borchers, C. Chang, C. L. Keen, M. E. Gershwin, Idiopathic pulmonary fibrosis—An epidemiological and pathological review. *Clin. Rev. Allergy Immunol.* **40**, 117–134 (2011).
8. C. G. Lee, R. J. Homer, Z. Zhu, S. Lanone, X. Wang, V. Koteliansky, J. M. Shipley, P. Gotwals, P. Noble, Q. Chen, R. M. Senior, J. A. Elias, Interleukin-13 induces tissue fibrosis by selectively stimulating and activating transforming growth factor β_1. *J. Exp. Med.* **194**, 809–822 (2001).
9. P. Pakshir, B. Hinz, The big five in fibrosis: Macrophages, myofibroblasts, matrix, mechanics, and miscommunication. *Matrix Biol.* **68–69**, 81–93 (2018).
10. P. Sivakumar, P. Ntolios, G. Jenkins, G. Laurent, Into the matrix: Targeting fibroblasts in pulmonary fibrosis. *Curr. Opin. Pulm. Med.* **18**, 462–469 (2012).
11. D. L. Clarke, A. M. Carruthers, T. Mustelin, L. A. Murray, Matrix regulation of idiopathic pulmonary fibrosis: The role of enzymes. *Fibrog. Tissue Repair* **6**, 20 (2013).
12. A. U. Wells, C. P. Denton, Interstitial lung disease in connective tissue disease—Mechanisms and management. *Nat. Rev. Rheumatol.* **10**, 728–739 (2014).
13. N. Ahluwalia, B. S. Shea, A. M. Tager, New therapeutic targets in idiopathic pulmonary fibrosis. Aiming to rein in runaway wound-healing responses. *Am. J. Respir. Crit. Care Med.* **190**, 867–878 (2014).
14. C. E. Barkauskas, P. W. Noble, Cellular mechanisms of tissue fibrosis. 7. New insights into the cellular mechanisms of pulmonary fibrosis. *Am. J. Physiol. Cell Physiol.* **306**, C987–C996 (2014).
15. I. Hoffmann, R. Balling, Cloning and expression analysis of a novel mesodermally expressed cadherin. *Dev. Biol.* **169**, 337–346 (1995).
16. L. Simonneau, M. Kitagawa, S. Suzuki, J. P. Thiery, Cadherin 11 expression marks the mesenchymal phenotype: Towards new functions for cadherins? *Cell Adhes. Commun.* **3**, 115–130 (1995).
17. S. Alimperti, S. T. Andreadis, CDH2 and CDH11 act as regulators of stem cell fate decisions. *Stem Cell Res.* **14**, 270–282 (2015).
18. M. Orlandini, S. Oliviero, In fibroblasts *Vegf-D* expression is induced by cell-cell contact mediated by cadherin-11. *J. Biol. Chem.* **276**, 6576–6581 (2001).
19. S. H. Richardson, T. Starborg, Y. Lu, S. M. Humphries, R. S. Meadows, K. E. Kadler, Tendon development requires regulation of cell condensation and cell shape via cadherin-11-mediated cell-cell junctions. *Mol. Cell. Biol.* **27**, 6218–6228 (2007).
20. B. Hinz, P. Pittet, J. Smith-Clerc, C. Chaponnier, J.-J. Meister, Myofibroblast development is characterized by specific cell-cell adherens junctions. *Mol. Biol. Cell* **15**, 4310–4320 (2004).
21. D. M. Lee, H. P. Kiener, S. K. Agarwal, E. H. Noss, G. F. M. Watts, O. Chisaka, M. Takeichi, M. B. Brenner, Cadherin-11 in synovial lining formation and pathology in arthritis. *Science* **315**, 1006–1010 (2007).
22. K. Tomita, A. van Bokhoven, G. J. L. H. van Leenders, E. T. G. Ruijter, C. F. J. Jansen, M. J. G. Bussemakers, J. A. Schalken, Cadherin switching in human prostate cancer progression. *Cancer Res.* **60**, 3650–3654 (2000).
23. T. Shibata, A. Ochiai, M. Gotoh, R. Machinami, S. Hirohashi, Simultaneous expression of cadherin-11 in signet-ring cell carcinoma and stromal cells of diffuse-type gastric cancer. *Cancer Lett.* **99**, 147–153 (1996).
24. S. K. Masur, R. J. Conors Jr., J. K. Cheung, S. Antohi, Matrix adhesion characteristics of corneal myofibroblasts. *Invest. Ophthalmol. Vis. Sci.* **40**, 904–910 (1999).
25. K. A. Kuijpers, J. P. Heesakkers, C. F. Jansen, J. A. Schalken, Cadherin-11 is expressed in detrusor smooth muscle cells and myofibroblasts of normal human bladder. *Eur. Urol.* **52**, 1213–1221 (2007).
26. S. K. Agarwal, Integrins and cadherins as therapeutic targets in fibrosis. *Front. Pharmacol.* **5**, 131 (2014).
27. D. J. Schneider, M. Wu, T. T. Le, S.-H. Cho, M. B. Brenner, M. R. Blackburn, S. K. Agarwal, Cadherin-11 contributes to pulmonary fibrosis: Potential role in TGF-β production and epithelial to mesenchymal transition. *FASEB J.* **26**, 503–512 (2012).
28. M. Black, D. Milewski, T. Le, X. Ren, Y. Xu, V. V. Kalinichenko, T. V. Kalin, FOXF1 inhibits pulmonary fibrosis by preventing CDH2-CDH11 cadherin switch in myofibroblasts. *Cell Rep.* **23**, 442–458 (2018).
29. M. Wu, M. Pedroza, R. Lafyatis, A.-T. George, M. D. Mayes, S. Assassi, F. K. Tan, M. B. Brenner, S. K. Agarwal, Identification of cadherin 11 as a mediator of dermal fibrosis and possible role in systemic sclerosis. *Arthritis Rheumatol.* **66**, 1010–1021 (2014).
30. F. Strutz, M. Zeisberg, F. N. Ziyadeh, C. Q. Yang, R. Kalluri, G. A. Müller, E. G. Neilson, A. Renziehausen, Z. Sisic, Role of basic fibroblast growth factor-2 in epithelial-mesenchymal transformation. *Kidney Int.* **61**, 1714–1728 (2002).
31. J. D. Hutcheson, J. Chen, M. K. Sewell-Loftin, L. M. Ryzhova, C. I. Fisher, Y. R. Su, W. D. Merryman, Cadherin-11 regulates cell–cell tension necessary for calcific nodule formation by valvular myofibroblasts. *Arterioscler. Thromb. Vasc. Biol.* **33**, 114–120 (2013).
32. H. Wang, L. A. Leinwand, K. S. Anseth, Roles of transforming growth factor-β1 and OB-cadherin in porcine cardiac valve myofibroblast differentiation. *FASEB J.* **28**, 4551–4562 (2014).
33. J. S. N. Verhoekx, L. S. Verjee, D. Izadi, J. K. K. Chan, V. Nicolaidou, D. Davidson, K. S. Midwood, J. Nanchahal, Isometric contraction of Dupuytren's myofibroblasts is inhibited by blocking intercellular junctions. *J. Invest. Dermatol.* **133**, 2664–2671 (2013).
34. X. Valencia, J. M. G. Higgins, H. P. Kiener, D. M. Lee, T. A. Podrebarac, C. C. Dascher, G. F. M. Watts, E. Mizoguchi, B. Simmons, D. D. Patel, A. K. Bhan, M. B. Brenner, Cadherin-11 provides specific cellular adhesion between fibroblast-like synoviocytes. *J. Exp. Med.* **200**, 1673–1679 (2004).
35. A. Mantovani, S. K. Biswas, M. R. Galdiero, A. Sica, M. Locati, Macrophage plasticity and polarization in tissue repair and remodelling. *J. Pathol.* **229**, 176–185 (2013).
36. T. A. Wynn, A. Chawla, J. W. Pollard, Macrophage biology in development, homeostasis and disease. *Nature* **496**, 445–455 (2013).

Downloaded from http://stke.sciencemag.org/ on January 15, 2019

37. R. J. Snyder, J. Lantis, R. S. Kirsner, V. Shah, M. Molyneaux, M. J. Carter, Macrophages: A review of their role in wound healing and their therapeutic use. *Wound Repair Regen.* **24**, 613–629 (2016).
38. S. A. Eming, P. Martin, M. Tomic-Canic, Wound repair and regeneration: Mechanisms, signaling, and translation. *Sci. Transl. Med.* **6**, 265sr6 (2014).
39. R. K. Assoian, B. E. Fleurdelys, H. C. Stevenson, P. J. Miller, D. K. Madtes, E. W. Raines, R. Ross, M. B. Sporn, Expression and secretion of type beta transforming growth factor by activated human macrophages. *Proc. Natl. Acad. Sci. U.S.A.* **84**, 6020–6024 (1987).
40. H. Chong, Y. Vodovotz, G. W. Cox, M. H. Barcellos-Hoff, Immunocytochemical localization of latent transforming growth factor-β1 activation by stimulated macrophages. *J. Cell. Physiol.* **178**, 275–283 (1999).
41. I. Nunes, R. L. Shapiro, D. B. Rifkin, Characterization of latent TGF-beta activation by murine peritoneal macrophages. *J. Immunol.* **155**, 1450–1459 (1995).
42. D. R. Twardzik, J. A. Mikovits, J. E. Ranchalis, A. F. Purchio, L. Ellingsworth, F. W. Ruscetti, γ-Interferon-induced activation of latent transforming growth factor-β by human monocytes. *Ann. N. Y. Acad. Sci.* **593**, 276–284 (1990).
43. S. W. Glasser, J. S. Hagood, S. Wong, C. A. Taype, S. K. Madala, W. D. Hardie, Mechanisms of lung fibrosis resolution. *Am. J. Pathol.* **186**, 1066–1077 (2016).
44. A. J. Lechner, I. H. Driver, J. Lee, C. M. Conroy, A. Nagle, R. M. Locksley, J. R. Rock, Recruited monocytes and type 2 immunity promote lung regeneration following pneumonectomy. *Cell Stem Cell* **21**, 120–134.e7 (2017).
45. Z. Zhu, J. Ding, Z. Ma, T. Iwashina, E. E. Tredget, Systemic depletion of macrophages in the subacute phase of wound healing reduces hypertrophic scar formation. *Wound Repair Regen.* **24**, 644–656 (2016).
46. M. A. Gibbons, A. C. MacKinnon, P. Ramachandran, K. Dhaliwal, R. Duffin, A. T. Phythian-Adams, N. van Rooijen, C. Haslett, S. E. Howie, A. J. Simpson, N. Hirani, J. Gauldie, J. P. Iredale, T. Sethi, S. J. Forbes, Ly6Chi monocytes direct alternatively activated profibrotic macrophage regulation of lung fibrosis. *Am. J. Respir. Crit. Care Med.* **184**, 569–581 (2011).
47. L. A. Murray, Q. Chen, M. S. Kramer, D. P. Hesson, R. L. Argentieri, X. Peng, M. Gulati, R. J. Homer, T. Russell, N. van Rooijen, J. A. Elias, C. M. Hogaboam, E. L. Herzog, TGF-beta driven lung fibrosis is macrophage dependent and blocked by serum amyloid P. *Int. J. Biochem. Cell Biol.* **43**, 154–162 (2011).
48. J. S. Duffield, S. J. Forbes, C. M. Constandinou, S. Clay, M. Partolina, S. Vuthoori, S. Wu, R. Lang, J. P. Iredale, Selective depletion of macrophages reveals distinct, opposing roles during liver injury and repair. *J. Clin. Invest.* **115**, 56–65 (2005).
49. J. M. Fritz, M. A. Tennis, D. J. Orlicky, H. Yin, C. Ju, E. F. Redente, K. S. Choo, T. A. Staab, R. J. Bouchard, D. T. Merrick, A. M. Malkinson, L. D. Dwyer-Nield, Depletion of tumor-associated macrophages slows the growth of chemically induced mouse lung adenocarcinomas. *Front. Immunol.* **5**, 587 (2014).
50. T. Lucas, A. Waisman, R. Ranjan, J. Roes, T. Krieg, W. Muller, A. Roers, S. A. Eming, Differential roles of macrophages in diverse phases of skin repair. *J. Immunol.* **184**, 3964–3977 (2010).
51. S. Gordon, Alternative activation of macrophages. *Nat. Rev. Immunol.* **3**, 23–35 (2003).
52. P. J. Murray, J. E. Allen, S. K. Biswas, E. A. Fisher, D. W. Gilroy, S. Goerdt, S. Gordon, J. A. Hamilton, L. B. Ivashkiv, T. Lawrence, M. Locati, A. Mantovani, F. O. Martinez, J.-L. Mege, D. M. Mosser, G. Natoli, J. P. Saeij, J. L. Schultze, K. A. Shirey, A. Sica, J. Suttles, I. Udalova, J. A. van Ginderachter, S. N. Vogel, T. A. Wynn, Macrophage activation and polarization: Nomenclature and experimental guidelines. *Immunity* **41**, 14–20 (2014).
53. C. Varol, A. Mildner, S. Jung, Macrophages: Development and tissue specialization. *Annu. Rev. Immunol.* **33**, 643–675 (2015).
54. C. K. Glass, N. Natoli, Molecular control of activation and priming in macrophages. *Nat. Immunol.* **17**, 26–33 (2016).
55. A. Sica, A. Mantovani, Macrophage plasticity and polarization: In vivo veritas. *J. Clin. Invest.* **122**, 787–795 (2012).
56. M. P. Motwani, D. W. Gilroy, Macrophage development and polarization in chronic inflammation. *Semin. Immunol.* **27**, 257–266 (2015).
57. L. C. Davies, S. J. Jenkins, J. E. Allen, P. R. Taylor, Tissue-resident macrophages. *Nat. Immunol.* **14**, 986–995 (2013).
58. D. M. Mosser, J. P. Edwards, Exploring the full spectrum of macrophage activation. *Nat. Rev. Immunol.* **8**, 958–969 (2008).
59. W. M. Brieher, A. S. Yap, Cadherin junctions and their cytoskeleton(s). *Curr. Opin. Cell Biol.* **25**, 39–46 (2013).
60. P. Pittet, K. Lee, A. J. Kulik, J.-J. Meister, B. Hinz, Fibrogenic fibroblasts increase intercellular adhesion strength by reinforcing individual OB-cadherin bonds. *J. Cell Sci.* **121**, 877–886 (2008).
61. E. B. Meltzer, W. T. Barry, T. A. D'Amico, R. D. Davis, S. S. Lin, M. W. Onaitis, L. D. Morrison, T. A. Sporn, M. P. Steele, P. W. Noble, Bayesian probit regression model for the diagnosis of pulmonary fibrosis: Proof-of-principle. *BMC Med. Genenomics* **4**, 70 (2011).
62. X. Peng, M. Moore, A. Mathur, Y. Zhou, H. Sun, Y. Gan, J. D. Herazo-Maya, N. Kaminski, X. Hu, H. Pan, C. Ryu, A. Osafo-Addo, R. J. Homer, C. Feghali-Bostwick, W. H. Fares, M. Gulati, B. Hu, C.-G. Lee, J. A. Elias, E. L. Herzog, Plexin C1 deficiency permits synaptotagmin 7–mediated macrophage migration and enhances mammalian lung fibrosis. *FASEB J.* **30**, 4056–4070 (2016).
63. Y. Bauer, J. Tedrow, S. de Bernard, M. Birker-Robaczewska, K. F. Gibson, B. J. Guardela, P. Hess, A. Klenk, K. O. Lindell, S. Poirey, B. Renault, M. Rey, E. Weber, O. Nayler, N. Kaminski, A novel genomic signature with translational significance for human idiopathic pulmonary fibrosis. *Am. J. Respir. Cell Mol. Biol.* **52**, 217–231 (2015).
64. S. Cabrera, M. Selman, A. Lonzano-Bolaños, K. Konishi, T. J. Richards, N. Kaminski, A. Pardo, Gene expression profiles reveal molecular mechanisms involved in the progression and resolution of bleomycin-induced lung fibrosis. *Am. J. Physiol. Lung Cell. Mol. Physiol.* **304**, L593–L601 (2013).
65. J. L. Balestrini, S. Chaudhry, V. Sarrazy, A. Koehler, B. Hinz, The mechanical memory of lung myofibroblasts. *Integr. Biol.* **4**, 410–421 (2012).
66. M. Nahrendorf, F. K. Swirski, Abandoning M1/M2 for a network model of macrophage function. *Circ. Res.* **119**, 414–417 (2016).
67. S. J. Forbes, N. Rosenthal, Preparing the ground for tissue regeneration: From mechanism to therapy. *Nat. Med.* **20**, 857–869 (2014).
68. B. Hinz, G. Celetta, J. J. Tomasek, G. Gabbiani, C. Chaponnier, Alpha-smooth muscle actin expression upregulates fibroblast contractile activity. *Mol. Biol. Cell* **12**, 2730–2741 (2001).
69. P.-J. Wipff, D. B. Rifkin, J.-J. Meister, B. Hinz, Myofibroblast contraction activates latent TGF-β1 from the extracellular matrix. *J. Cell Biol.* **179**, 1311–1323 (2007).
70. F. Klingberg, G. Chau, M. Walraven, S. Boo, A. Koehler, M. L. Chow, A. L. Olsen, M. Im, M. Lodyga, R. G. Wells, E. S. White, B. Hinz, The fibronectin ED-A domain enhances recruitment of latent TGF-β-binding protein-1 to the fibroblast matrix. *J. Cell Sci.* **131**, jcs201293 (2018).
71. B. Hinz, It has to be the αv: Myofibroblast integrins activate latent TGF-β1. *Nat. Med.* **19**, 1567–1568 (2013).
72. N. C. Henderson, D. Sheppard, Integrin-mediated regulation of TGFβ in fibrosis. *Biochim. Biophys. Acta* **1832**, 891–896 (2013).
73. L. Follonier, S. Schaub, J.-J. Meister, B. Hinz, Myofibroblast communication is controlled by intercellular mechanical coupling. *J. Cell Sci.* **121**, 3305–3316 (2008).
74. S. Row, Y. Liu, S. Alimperti, S. K. Agarwal, S. T. Andreadis, Cadherin-11 is a novel regulator of extracellular matrix synthesis and tissue mechanics. *J. Cell Sci.* **129**, 2950–2961 (2016).
75. R. P. Langhe, T. Gudzenko, M. Bachmann, S. F. Becker, C. Gonnermann, C. Winter, G. Abbruzzese, D. Alfandari, M.-C. Kratzer, C. M. Franz, J. Kashef, Cadherin-11 localizes to focal adhesions and promotes cell-substrate adhesion. *Nat. Commun.* **7**, 10909 (2016).
76. S. Alimperti, H. You, T. George, S. K. Agarwal, S. T. Andreadis, Cadherin-11 regulates both mesenchymal stem cell differentiation into smooth muscle cells and the development of contractile function in vivo. *J. Cell Sci.* **127**, 2627–2638 (2014).
77. Z. Zhu, J. Ding, Z. Ma, T. Iwashina, E. E. Tredget, Alternatively activated macrophages derived from THP-1 cells promote the fibrogenic activities of human dermal fibroblasts. *Wound Repair Regen.* **25**, 377–388 (2017).
78. H. E. Mewhort, B. D. Lipon, D. A. Svystonyuk, G. Teng, D. G. Guzzardi, C. Silva, V. W. Yong, P. W. M. Fedak, Monocytes increase human cardiac myofibroblast-mediated extracellular matrix remodeling through TGF-β1. *Am. J. Physiol. Heart Circ. Physiol.* **310**, H716–H724 (2016).
79. X. Zhou, R. A. Franklin, M. Adler, J. B. Jacox, W. Bailis, J. A. Shyer, R. A. Flavell, A. Mayo, U. Alon, R. Medzhitov, Circuit design features of a stable two-cell system. *Cell* **172**, 744–757.e17 (2018).
80. T. A. Wynn, L. Barron, Macrophages: Master regulators of inflammation and fibrosis. *Semin. Liver Dis.* **30**, 245–257 (2010).
81. R. Mori, T. J. Shaw, P. Martin, Molecular mechanisms linking wound inflammation and fibrosis: Knockdown of osteopontin leads to rapid repair and reduced scarring. *J. Exp. Med.* **205**, 43–51 (2008).
82. J. L. Cash, M. D. Bass, J. Campbell, M. Barnes, P. Kubes, P. Martin, Resolution mediator chemerin15 reprograms the wound microenvironment to promote repair and reduce scarring. *Curr. Biol.* **24**, 1406–1414 (2014).
83. J. A. Knipper, S. Willenborg, J. Brinckmann, W. Bloch, T. Maaß, R. Wagener, T. Krieg, T. Sutherland, A. Munitz, M. E. Rothenberg, A. Niehoff, R. Richardson, M. Hammerschmidt, J. E. Allen, S. A. Eming, Interleukin-4 receptor α signaling in myeloid cells controls collagen fibril assembly in skin repair. *Immunity* **43**, 803–816 (2015).
84. D. T. Ploeger, N. A. Hosper, M. Schipper, J. A. Koerts, S. de Rond, R. A. Bank, Cell plasticity in wound healing: Paracrine factors of M1/ M2 polarized macrophages influence the phenotypical state of dermal fibroblasts. *Cell Commun. Signal.* **11**, 29 (2013).
85. S. M. Wahl, N. McCartney-Francis, J. B. Allen, E. B. Dougherty, S. F. Dougherty, Macrophage production of TGF-β and regulation by TGF- β. *Ann. N. Y. Acad. Sci.* **593**, 188–196 (1990).
86. A. Antonelli-Orlidge, K. B. Saunders, S. R. Smith, P. A. D'Amore, An activated form of transforming growth factor beta is produced by cocultures of endothelial cells and pericytes. *Proc. Natl. Acad. Sci. U.S.A.* **86**, 4544–4548 (1989).

Downloaded from http://stke.sciencemag.org/ on January 15, 2019

87. Y. Sato, D. B. Rifkin, Inhibition of endothelial cell movement by pericytes and smooth muscle cells: Activation of a latent transforming growth factor-beta 1-like molecule by plasmin during coculture. *J. Cell Biol.* **109**, 309–315 (1989).
88. J. S. Munger, X. Huang, H. Kawakatsu, M. J. D. Griffiths, S. L. Dalton, J. Wu, J. F. Pittet, N. Kaminski, C. Garat, M. A. Matthay, D. B. Rifkin, D. Sheppard, The integrin alpha v beta 6 binds and activates latent TGF beta 1: A mechanism for regulating pulmonary inflammation and fibrosis. *Cell* **96**, 319–328 (1999).
89. X. Dong, B. Zhao, R. E. Iacob, J. Zhu, A. C. Koksal, C. Lu, J. R. Engen, T. A. Springer, Force interacts with macromolecular structure in activation of TGF-β. *Nature* **542**, 55–59 (2017).
90. L. Buscemi, D. Ramonet, F. Klingberg, A. Formey, J. Smith-Clerc, J. J. Meister, B. Hinz, The single-molecule mechanics of the latent TGF-β1 complex. *Curr. Biol.* **21**, 2046–2054 (2011).
91. N. C. Henderson, T. D. Arnold, Y. Katamura, M. M. Giacomini, J. D. Rodriguez, J. H. McCarty, A. Pellicoro, E. Raschperger, C. Betsholtz, P. G. Ruminski, D. W. Griggs, M. J. Prinsen, J. J. Maher, J. P. Iredale, A. Lacy-Hulbert, R. H. Adams, D. Sheppard, Targeting of α_v integrin identifies a core molecular pathway that regulates fibrosis in several organs. *Nat. Med.* **19**, 1617–1624 (2013).
92. N. I. Reed, H. Jo, C. Chen, K. Tsujino, T. D. Arnold, W. F. DeGrado, D. Sheppard, The αvβ1 integrin plays a critical in vivo role in tissue fibrosis. *Sci. Transl. Med.* **7**, 288ra79 (2015).
93. A. W. Taylor, Review of the activation of TGF-β in immunity. *J. Leukoc. Biol.* **85**, 29–33 (2009).
94. M. A. Travis, D. Sheppard, TGF-β activation and function in immunity. *Annu. Rev. Immunol.* **32**, 51–82 (2014).
95. G. Gabriely, A. P. da Cunha, R. M. Rezende, B. Kenyon, A. Madi, T. Vandeventer, N. Skillin, S. Rubino, L. Garo, M. A. Mazzola, P. Kolypetri, A. J. Lanser, T. Moreira, A. M. C. Faria, H. Lassmann, V. Kuchroo, G. Murugaiyan, H. L. Weiner, Targeting latency-associated peptide promotes antitumor immunity. *Sci. Immunol.* **2**, eaaj1738 (2017).
96. J. Stockis, S. Liénart, D. Colau, A. Collignon, S. L. Nishimura, D. Sheppard, P. G. Coulie, S. Lucas, Blocking immunosuppression by human Tregs in vivo with antibodies targeting integrin αVβ8. *Proc. Natl. Acad. Sci. U.S.A.* **114**, E10161–E10168 (2017).
97. J. Stockis, O. Dedobbeleer, S. Lucas, Role of GARP in the activation of latent TGF-β1. *Mol. Biosyst.* **13**, 1925–1935 (2017).
98. S. Lienart, J. Stockis, O. Dedobbeleer, S. Lucas, Targeting immunosuppression by Tregs with monoclonal antibodies against GARP. *Oncoimmunology* **5**, e1074379 (2016).
99. S. A. Hahn, A. Neuhoff, J. Landsberg, J. Schupp, D. Eberts, P. Leukel, M. Bros, M. Weilbaecher, D. Schuppan, S. Grabbe, T. Tueting, V. Lennerz, C. Sommer, H. Jonuleit, A. Tuettenberg, A key role of GARP in the immune suppressive tumor microenvironment. *Oncotarget* **7**, 42996–43009 (2016).
100. S. Rachidi, A. Metelli, B. Riesenberg, B. X. Wu, M. H. Nelson, C. Wallace, C. M. Paulos, M. P. Rubinstein, E. Garrett-Mayer, M. Hennig, D. W. Bearden, Y. Yang, B. Liu, Z. Li, Platelets subvert T cell immunity against cancer via GARP-TGFβ axis. *Sci. Immunol.* **2**, eaai7911 (2017).
101. Y. Qin, B. S. Garrison, W. Ma, R. Wang, A. Jiang, J. Li, M. Mistry, R. T. Bronson, D. Santoro, C. Franco, D. A. Robinton, B. Stevens, D. J. Rossi, C. Lu, T. A. Springer, A milieu molecule for TGF-β required for microglia function in the nervous system. *Cell* **174**, 156–171.e16 (2018).
102. C. Godbout, L. Follonier Castella, E. A. Smith, N. Talele, M. L. Chow, A. Garonna, B. Hinz, The mechanical environment modulates intracellular calcium oscillation activities of myofibroblasts. *PLOS ONE* **8**, e64560 (2013).
103. J. M. Goffin, P. Pittet, G. Csucs, J. W. Lussi, J.-J. Meister, B. Hinz, Focal adhesion size controls tension-dependent recruitment of alpha-smooth muscle actin to stress fibers. *J. Cell Biol.* **172**, 259–268 (2006).
104. F. Klingberg, M. L. Chow, A. Koehler, S. Boo, L. Buscemi, T. M. Quinn, M. Costell, B. A. Alman, E. Genot, B. Hinz, Prestress in the extracellular matrix sensitizes latent TGF-β1 for activation. *J. Cell Biol.* **207**, 283–297 (2014).
105. S. K. Chang, A. C. Kohlgruber, F. Mizoguchi, X. Michelet, B. J. Wolf, K. Wei, P. Y. Lee, L. Lynch, D. Duquette, V. Ceperuelo-Mallafré, A. S. Banks, M. B. Brenner, Stromal cell cadherin-11 regulates adipose tissue inflammation and diabetes. *J. Clin. Invest.* **127**, 3300–3312 (2017).
106. R. G. Jenkins, B. B. Moore, R. C. Chambers, O. Eickelberg, M. Königshoff, M. Kolb, G. J. Laurent, C. B. Nanthakumar, M. A. Olman, A. Pardo, M. Selman, D. Sheppard, P. J. Sime, A. M. Tager, A. L. Tatler, V. J. Thannickal, E. S. White; ATS Assembly on Respiratory Cell and Molecular Biology, An official American Thoracic Society workshop report: Use of animal models for the preclinical assessment of potential therapies for pulmonary fibrosis. *Am. J. Respir. Cell Mol. Biol.* **56**, 667–679 (2017).
107. E. A. Ayaub, P. S. Kolb, Z. Mohammed-Ali, V. Tat, J. Murphy, P.-S. Bellaye, C. Shimbori, F. J. Boivin, R. Lai, E. G. Lynn, Š. Lhoták, D. Bridgewater, M. R. J. Kolb, M. D. Inman, J. G. Dickhout, R. C. Austin, K. Ask, GRP78 and CHOP modulate macrophage apoptosis and the development of bleomycin-induced pulmonary fibrosis. *J. Pathol.* **239**, 411–425 (2016).
108. C. X. Li, N. P. Talele, S. Boo, A. Koehler, E. Knee-Walden, J. L. Balestrini, P. Speight, A. Kapus, B. Hinz, MicroRNA-21 preserves the fibrotic mechanical memory of mesenchymal stem cells. *Nat. Mater.* **16**, 379–389 (2016).
109. S. K. Chang, E. H. Noss, M. Chen, Z. Gu, K. Townsend, R. Grenha, L. Leon, S. Y. Lee, D. M. Lee, M. B. Brenner, Cadherin-11 regulates fibroblast inflammation. *Proc. Natl. Acad. Sci. U.S.A.* **108**, 8402–8407 (2011).
110. C. M. Counter, W. C. Hahn, W. Wei, S. D. Caddle, R. L. Beijersbergen, P. M. Lansdorp, J. M. Sedivy, R. A. Weinberg, Dissociation among in vitro telomerase activity, telomere maintenance, and cellular immortalization. *Proc. Natl. Acad. Sci. U.S.A.* **95**, 14723–14728 (1998).
111. M. Abe, J. G. Harpel, C. N. Metz, I. Nunes, D. J. Loskutoff, D. B. Rifkin, An assay for transforming growth factor-β using cells transfected with a plasminogen activator inhibitor-1 promoter-luciferase construct. *Anal. Biochem.* **216**, 276–284 (1994).
112. E. A. Ayaub, A. Dubey, J. Imani, F. Botelho, M. R. J. Kolb, C. D. Richards, K. Ask, Overexpression of OSM and IL-6 impacts the polarization of pro-fibrotic macrophages and the development of bleomycin-induced lung fibrosis. *Sci. Rep.* **7**, 1E3281 (2017).
113. M. W. Pfaffl, A new mathematical model for relative quantification in real-time RT-PCR. *Nucleic Acids Res.* **29**, e45 (2001).

Acknowledgments: We thank C. Chaponnier and G. Gabbiani (University of Geneva, Switzerland) for providing antibodies directed against α-SMA and M. Brenner (Harvard Medical School) for providing CDH11 function–blocking antibodies. We thank the staff of the Electron microscopy laboratory (Biocenter Oulu) and D. Holmyard at the SickKids Biomedical Nanoscale Imaging Facility (Toronto) for technical support and expert advice. We are grateful to K. Tandon, N. Hambly, A. Naqvi, J. C. Cutz, and A. Ayoub at the Firestone Institute for Respiratory Health, Department of Medicine, McMaster University, Hamilton, ON, Canada for contributing to the conception and design of the human tissue microarray, as well as the selection of the tissues on the basis of patient's clinical history and pathologic/histologic outcomes. We thank E. Ayaub (McMaster University, Hamilton, Canada) for continuous help and advice throughout the project; C. Spring, C. Di Ciano-Oliveira, and P. Plant from the Research Core Facility at the Keenan Research Centre, St. Michael's Hospital for valuable technical support; A. Boczula and T. Moriarty (Faculty of Dentistry, Toronto) for indispensable guidance and advice in generating the hTERT immortalized cell line; and M. Im for help in creating the schema. **Funding**: This research was supported by the Canadian Institutes of Health Research (CIHR) (grant nos. 137060, 286920, 286720, and 375597), the Collaborative Health Research Programme (CIHR/NSERC grant no. 413783), the Canada Foundation for Innovation and Ontario Research Fund (CFI/ORF grant nos. 26653 and 503465), and the E-Rare Joint Transnational Program "Development of Innovative Therapeutic Approaches for Rare Diseases" (grant no. ERL-138395) (all to B.H.). M.K. received funding by the Campaign to Cure Arthritis via the Toronto General and Western Hospital Foundation, University Health Network, Toronto. R.K. received support from the Foundation of the Finnish Anti-tuberculosis Association, a state subsidy of Oulu University Hospital and the Health Care Foundation of North Finland. K.A. was funded by the Ontario Thoracic Society (Canadian Lung Association). H.M.K. was receiving fellowship support from The Academy of Finland (grant no. 285835). **Author contributions**: E.C., M.L., P.P., H.M.K., B.W., M. Kiebalo, and S.B. performed experiments and analyzed data. M.G., R.K., M. Kapoor, and K.A. performed or supervised select experiments and generated reagents for the study. B.H. designed and supervised the study and drafted the manuscript; all authors contributed to manuscript writing and editing. **Competing interests:** The authors declare that they have no competing interests. **Data and materials availability**: All data needed to evaluate the conclusions in the paper are present in the paper or the Supplementary Materials.

Submitted 10 July 2017
Accepted 17 December 2018
Published 15 January 2019
10.1126/scisignal.aao3469

Citation: M. Lodyga, E. Cambridge, H. M. Karvonen, P. Pakshir, B. Wu, S. Boo, M. Kiebalo, R. Kaarteenaho, M. Glogauer, M. Kapoor, K. Ask, B. Hinz, Cadherin-11–mediated adhesion of macrophages to myofibroblasts establishes a profibrotic niche of active TGF-β. *Sci. Signal.* **12**, eaao3469 (2019).

Downloaded from http://stke.sciencemag.org/ on January 15, 2019

Science Signaling

Cadherin-11–mediated adhesion of macrophages to myofibroblasts establishes a profibrotic niche of active TGF- β

Monika Lodyga, Elizabeth Cambridge, Henna M. Karvonen, Pardis Pakshir, Brian Wu, Stellar Boo, Melanie Kiebalo, Riitta Kaarteenaho, Michael Glogauer, Mohit Kapoor, Kjetil Ask and Boris Hinz

Sci. Signal. **12** (564), eaao3469.
DOI: 10.1126/scisignal.aao3469

Macrophage-myofibroblast adhesion creates a profibrotic niche

The reversible activation of fibroblasts into extracellular matrix–secreting myofibroblasts is a consequence of inflammation and is critical for wound healing and tissue repair; however, persistent myofibroblast activity causes fibrosis. Inflammatory macrophages produce transforming growth factor –β (TGF-β), a cytokine that induces the fibroblast-to-myofibroblast transition. Lodyga *et al.* found that the adhesion protein cadherin-11 (CDH11) was enriched at points of contact between macrophages and myofibroblasts in fibrotic lung tissues from mice and human patients. Cdh11-mediated adhesion between primary mouse macrophages and lung fibroblasts promoted the activation of fibroblasts into myofibroblasts and supported myofibroblast activity by acting as a local source of latent TGF- β that was activated by the myofibroblasts. Thus, Cdh11-mediated adhesion prolongs and targets the delivery of macrophage-produced TGF-β to myofibroblasts, creating a self-sustaining profibrotic niche.

ARTICLE TOOLS http://stke.sciencemag.org/content/12/564/eaao3469

SUPPLEMENTARY MATERIALS http://stke.sciencemag.org/content/suppl/2019/01/11/12.564.eaao3469.DC1

RELATED CONTENT
http://stke.sciencemag.org/content/sigtrans/10/506/eaao1822.full
http://stke.sciencemag.org/content/sigtrans/11/532/eaar2566.full
http://science.sciencemag.org/content/sci/356/6342/1026.full
http://science.sciencemag.org/content/sci/362/6417/eaar2971.full
http://stm.sciencemag.org/content/scitransmed/10/431/eaaf5307.full
http://stm.sciencemag.org/content/scitransmed/10/429/eaan0333.full
http://stm.sciencemag.org/content/scitransmed/9/420/eaal3765.full
http://stm.sciencemag.org/content/scitransmed/10/460/eaar8356.full
http://advances.sciencemag.org/content/advances/4/7/eaas9944.full

REFERENCES This article cites 113 articles, 33 of which you can access for free
http://stke.sciencemag.org/content/12/564/eaao3469#BIBL

PERMISSIONS http://www.sciencemag.org/help/reprints-and-permissions

Use of this article is subject to the Terms of Service

Science Signaling (ISSN 1937-9145) is published by the American Association for the Advancement of Science, 1200 New York Avenue NW, Washington, DC 20005. 2017 © The Authors, some rights reserved; exclusive licensee American Association for the Advancement of Science. No claim to original U.S. Government Works. The title *Science Signaling* is a registered trademark of AAAS.

Downloaded from http://stke.sciencemag.org/ on January 15, 2019